EES Batteries

REVIEW

View Article Online
View Journal

Open Access Article. Published on 23 December 2025. Downloaded on 1/13/2026 8:44:30 PM.
This article is licensed under a Creative Commons Attribution-NonCommercial 3.0 Unported Licence.

Check for updates

Cite this: DOI: 10.1039/d5eb00198f

A cross-scale collaborative design of copper current collectors for practical anode-free lithium metal batteries

Jiawang Feng,[a] Tianzhengyi Zhang,[a] Ming Liu,[a] Guoxing Tian,[a] Yuqian Fan,[a] Ailing Song,*[a] Guangjie Shao*[a,b] and Zhipeng Ma*[a,b]

Anode-free lithium metal batteries (AFLMBs) represent the pinnacle of next-generation energy storage, promising exceptional energy densities and seamless integration with existing manufacturing infrastructure. However, their commercialization is critically hindered by the uncontrollable lithium deposition behavior on the inherently lithiophobic copper current collector (Cu CC), leading to low coulombic efficiency, dendritic growth, and rapid failure. While extensive efforts have been dedicated to modifying the Cu CC, a fragmented view often prevails, lacking a unified design principle that bridges different scales. This review moves beyond conventional summaries by proposing a novel paradigm of cross-scale collaborative design. We construct a comprehensive strategic framework that systematically integrates modification strategies from the atomic/nano-scale (crystal facet engineering, artificial SEIs), through the micro-scale (3D porous, scaffold, and gradient structures), to the macro-scale (magnetic field introduction). A particular focus is placed on elucidating the synergistic mechanisms by which these multi-scale interventions collectively regulate the initial nucleation barrier, guide homogeneous Li^+ flux, and accommodate deposition-induced volume changes. Crucially, our analysis is consistently guided by the stringent performance benchmarks of the 'zero Li inventory' anode-free configuration, serving as a critical lens to assess the practical viability of each strategy. We further provide a forward-looking perspective on the fundamental challenges and scalable manufacturing pathways for translating these advanced current collectors from laboratory prototypes to industrial applications. This review aims to establish foundational design principles and inspire innovative solutions for developing practical high-energy-density lithium metal batteries.

Received 16th October 2025,
Accepted 21st December 2025

DOI: 10.1039/d5eb00198f

rsc.li/EESBatteries

Broader context

The global transition towards sustainable energy systems is critically dependent on the development of energy storage technologies with radically higher performance. While lithium-ion batteries have dominated the landscape, their energy density is approaching its theoretical limit, creating a pressing need for post-lithium-ion technologies. The anode-free lithium metal battery configuration, which maximizes energy density at the cell and system level by eliminating the initial anode host material, stands as the most promising candidate to power the next generation of electric vehicles and grid storage. However, the fundamental challenge of controlling lithium deposition on a bare current collector has hindered its practical realization, often leading to divergent research efforts focused on isolated solutions. This review provides a pivotal synthesis of these efforts by introducing a transformative *cross-scale collaborative design* philosophy. By constructing a unified framework that bridges atomic-level interactions, micro-scale architectures, and macro-scale physical fields, we move beyond incremental improvements to outline a coherent roadmap for engineering the ideal lithium metal host. Our work not only consolidates the state-of-the-art but also establishes a new paradigm for rational current collector design, aiming to accelerate the transition of anode-free batteries from a high-potential concept to a commercial reality that will underpin the future of electrified transportation and a resilient power grid.

1. Introduction

Fundamental shifts in the global energy architecture, propelled by the "dual-carbon" initiative, are intensifying performance requirements for next-generation storage technologies.[1–5] Electric vehicles, low-altitude aviation, and smart grids demand electrochemical systems with drastically improved

[a]Hebei Key Laboratory of Applied Chemistry, Hebei Key Laboratory of Heavy Metal Deep-Remediation in Water and Resource Reuse, School of Environmental and Chemical Engineering, Yanshan University, Qinhuangdao 066004, China. E-mail: ailing.song@ysu.edu.cn, shaoguangjie@ysu.edu.cn, mazp@ysu.edu.cn
[b]State Key Laboratory of Metastable Materials Science and Technology, Yanshan University, Qinhuangdao 066004, China

© 2026 The Author(s). Published by the Royal Society of Chemistry

Open Access Article. Published on 23 December 2025. Downloaded on 1/13/2026 8:44:30 PM.
This article is licensed under a Creative Commons Attribution-NonCommercial 3.0 Unported Licence.

energy densities, pushing conventional graphite-anode lithium-ion batteries toward their intrinsic limitations.[6–8] This impasse has renewed focus on lithium metal batteries (LMBs), recognized for their ultra-high theoretical energy density of ~500 Wh kg^{-1}. In particular, the anode-free lithium metal battery (AFLMB) configuration, which omits any initial anode lithium source, represents a critical advancement, achieving system-level energy densities exceeding 450 Wh kg^{-1} and positioning itself as a leading candidate for ultimate energy storage.[9–11]

Translating lithium metal anodes from concept to practical implementation, however, confronts persistent scientific barriers. The inherent high reactivity of lithium and unstable electrodeposition kinetics lead to continuous electrolyte decomposition, dendritic lithium formation, and a chronically unstable solid electrolyte interphase (SEI). This cascade rapidly depletes active lithium and electrolyte, causing poor coulombic efficiency, rapid capacity decay, and substantial safety concerns.[12–17]

Functional modification of the current collector has emerged as a pivotal approach to addressing these issues. Moving beyond its traditional role as a passive electron conductor and mechanical support, the current collector in AFLMBs acts as an active substrate. It defines the initial nucleation behavior and spatially guides lithium deposition; its surface properties critically influence nucleation barriers, deposit morphology, and interfacial integrity.[18] Commercial electrolytic copper foil, valued for its high conductivity, established processing technology, and robust mechanical properties, remains the most viable substrate. Yet its innate lithiophobicity, predominant (111) crystal faceting, and tendency to form a feeble native SEI contribute to a substantial nucleation overpotential (30–50 mV) and heterogeneous ion flux, initiating dendrite proliferation and accumulation of inactive lithium (Fig. 1).[19–22]

While surface engineering and three-dimensional structuring of copper current collectors represent active research fronts, existing reviews often concentrate on isolated tactics without a unified, application-oriented framework.[23–26] Many reported modifications are evaluated in cells with excess lithium, a condition starkly different from the "zero-lithium-inventory" reality in AFLMBs. Successful anode-free systems necessitate current collectors that achieve exceptional reversibility in the very first deposition/stripping cycle, demanding unprecedented precision and durability in their design.[27–30]

This review synthesizes prior research through an integrated "cross-scale" lens, examining functional copper collector design across atomic/nano (*e.g.*, crystallographic orientation, lithium-philic modification), micro (*e.g.*, artificial SEIs, porous scaffolds), and macro (*e.g.*, field-assisted) regimes (Fig. 2 and Table 1). We elucidate the interconnections and synergies among these strategies, detailing how they collectively guide initial nucleation, homogenize ion transport, and accommodate deposition-induced strain. By critically assessing their applicability toward the anode-free configuration, this analysis aims to establish foundational principles for developing practical, high-energy-density lithium metal batteries characterized by extended cycle life and intrinsic safety.

2. Surface engineering in two dimensions

In lithium-ion batteries, current collectors function primarily as electron transporters and physical supports for active materials, operating without direct contact with Li^+ ions or participation in faradaic reactions.[31,32] The paradigm shifts fundamentally in lithium metal batteries, where the current collector evolves from a passive conductor into an electrochemically active substrate—directly mediating lithium nucleation, guiding deposition morphology, and influencing interfacial evolution.[33,34] The initial nucleation behavior of lithium and the structure of the resulting solid electrolyte interphase (SEI) are decisive for deposition/stripping reversibility. Consequently, the nucleation barrier and microstructural

Jiawang Feng

Jiawang Feng is currently pursuing his Master's degree under the supervision of Professor Zhipeng Ma at the School of Environmental and Chemical Engineering, Yanshan University. His research interests mainly focus on the structural design of electrolytic copper foil and the development of novel electroplating solutions.

Ailing Song

Ailing Song is a Lecturer and Master's supervisor at the School of Environmental and Chemical Engineering, Yanshan University. She completed her Ph.D. in Chemical Engineering and Technology at Yanshan University in January 2021. From 2019 to 2021, she served as a visiting scholar at the University of Technology Sydney. Her research focuses on the design and development of highly stable advanced functional materials for energy storage and conversion applications.

© 2026 The Author(s). Published by the Royal Society of Chemistry

Open Access Article. Published on 23 December 2025. Downloaded on 1/13/2026 8:44:30 PM.
This article is licensed under a Creative Commons Attribution-NonCommercial 3.0 Unported Licence.

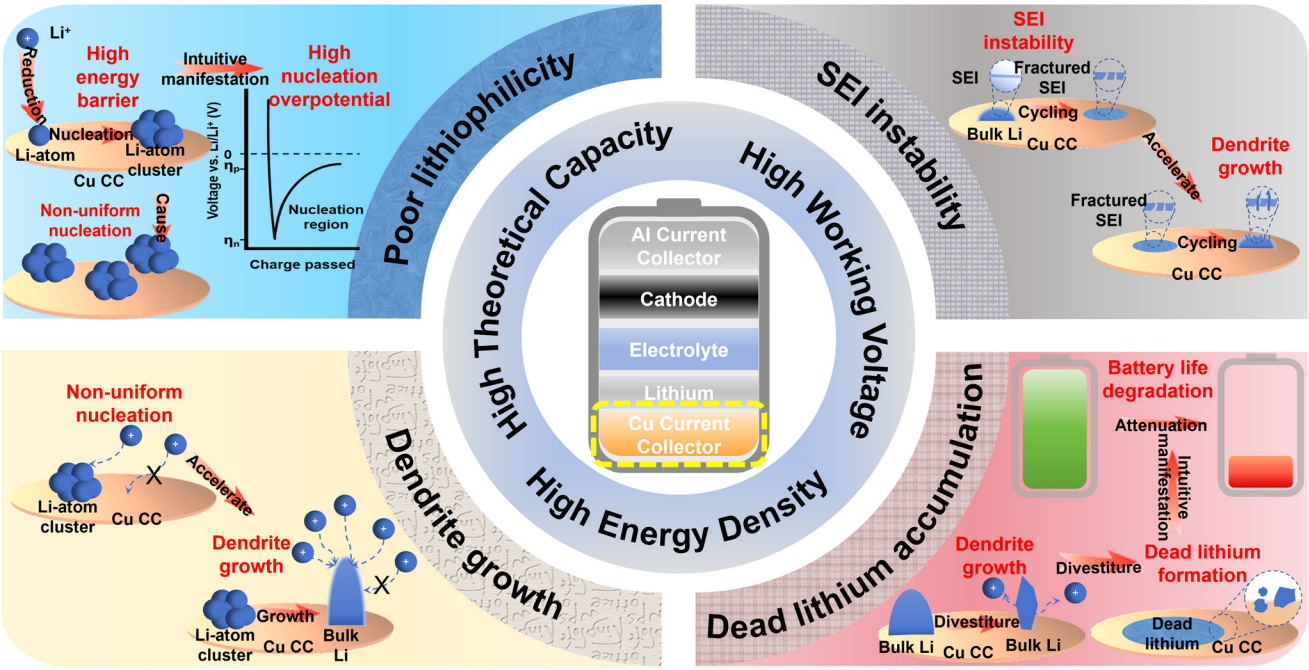

Fig. 1 Advantages of lithium metal batteries and issues when using electroplated copper foil as a lithium anode.

characteristics of the collector surface become critical determinants of cycling stability.[35,36] Plain commercial copper foil falls short of these requirements, making surface modification not merely beneficial but essential.[37]

2.1. Tailoring crystallographic orientation

According to classical heterogeneous nucleation theory, the nucleation size, morphology, and areal density of lithium on copper substrates are strongly influenced by the crystallographic orientation of the Cu surface.[38,39] Assuming minimal surface roughness, a smaller lattice mismatch reduces the interfacial contact angle (θ) and consequently the nucleation barrier. Simultaneously, a higher surface energy enhances the adsorption of Li adatoms, thereby facilitating nucleation (Fig. 3a).[40,41]

Conventional battery-grade copper foils are predominantly dominated by the (111) orientation. This facet exhibits a significant lattice mismatch with lithium and possesses the lowest surface energy among low-index Cu planes, impairing Li^+ adsorption. These factors collectively contribute to a high heterogeneous nucleation barrier, often initiating uneven lithium deposition and accelerating dendrite formation.[42,43]

Guangjie Shao

Guangjie Shao is a Professor and Ph.D. supervisor at the School of Environmental and Chemical Engineering, Yanshan University. He has worked as a member of the Hebei Key Laboratory of Applied Chemistry and the State Key Laboratory of Metastable Materials Science and Technology. He is an expert in electrochemistry and energy production, storage, and conversion. His primary research interests focus on addressing critical technical challenges associated with supercapacitors, metal–ion batteries, metal–sulfur batteries, and electrocatalysis, and developing high-gravity electrodeposition technology and nanostructured materials.

Zhipeng Ma

Zhipeng Ma, Professor and Ph.D. supervisor at the School of Environmental and Chemical Engineering, Yanshan University, earned his Ph.D. in Industrial Catalysis from Yanshan University in January 2015. His research focuses on the development of high-energy power batteries and the advancement of large-scale energy storage technologies, as well as lithium/sodium–ion batteries, lithium–sulfur batteries, large-scale aqueous energy storage systems, hydrogen production via water electrolysis, and the design and application of electrolytic metal foils.

Open Access Article. Published on 23 December 2025. Downloaded on 1/13/2026 8:44:30 PM.
This article is licensed under a Creative Commons Attribution-NonCommercial 3.0 Unported Licence.

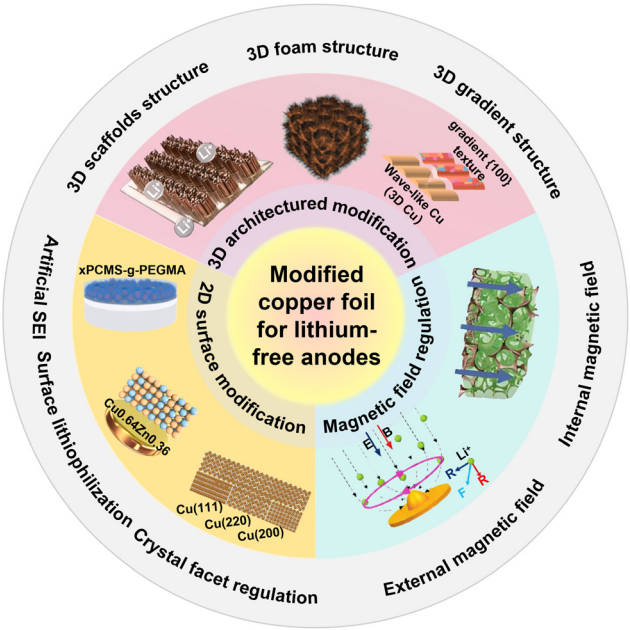

Fig. 2 Modification methods of copper foil.

DFT and AIMD simulations by Li *et al.* revealed that the Cu (110)@Li(100) interface demonstrates the smallest lattice mismatch (1.46%) and the highest binding energy (−0.99 J m^{-2}). The Cu(100)@Li(100) configuration also shows favorable characteristics, with a mismatch of 1.66% and a binding energy of −1.30 J m^{-2} (Fig. 3b).[44]

Controlling the preferential orientation of copper foil allows modulation of its surface free energy, enabling more controlled lithium deposition. Kim and colleagues discovered that Cu(100) single-crystal foil exhibits a lower Li nucleation overpotential compared to Cu(111) and Cu(110), with lithium preferentially adsorbing on Cu(100) regions (Fig. 3c). Their DFT calculations provided mechanistic insight: while Cu(110) shows the lowest Li adsorption barrier at low Li coverage, Cu (100) becomes more favorable under multi-layer Li adsorption conditions, with both significantly outperforming Cu(111) (Fig. 3d). Although a low adsorption barrier promotes lithium deposition, the Cu(110) surface is prone to passivation, which can impede subsequent lithium growth, leading to a higher observed nucleation overpotential compared to Cu(100).[45]

Building on this understanding, the team developed a copper current collector with a homogeneous (100) texture, achieving a tenfold increase in nucleation density and a twofold improvement in cycling stability.[46] In a complementary approach, Zhen *et al.* demonstrated that the FSI^- anion can direct the electrodeposition of copper ions along the (110) plane. The resulting highly (110)-oriented copper foil, employed in anode-free configurations, enabled uniform lithium deposition. When paired with an NCM811 cathode in a 350 Wh kg^{-1} pouch cell, the assembly retained 54.80% capacity after 100 cycles.[47]

Meanwhile, among the low-index Cu surfaces, the Cu(100) facet exhibits the strongest anion-binding capability. This tendency promotes substantial anion enrichment within the inner Helmholtz plane (IHP), which in turn facilitates the formation of an inorganic-rich SEI such as LiF and Li_3N, while improving both its mechanical robustness and the ionic transport characteristics. Experimental studies have shown that anions including FSI^- and $TFSI^-$ in ether-based electrolytes, as well as PF_6^- and ClO_4^- in ester-based systems, interact strongly with the Cu(100) surface, ultimately giving rise to a mechanically stiff and ionically conductive inorganic interphase.[48] In electrolyte systems with inherently higher anion concentrations, including localized high-concentration electrolytes (LHCE) and ionic liquids, the influence of such facet-dependent interactions is expected to be even more significant according to theoretical predictions. Nevertheless, direct experimental confirmation in these systems is still limited, indicating that further systematic investigation is required to fully elucidate these effects.

Collectively, both Cu(100) and Cu(110) facets offer superior lithiophilicity over Cu(111), attributed to their reduced lattice mismatch and elevated surface energy, leading to more homogeneous nucleation and enhanced cycling stability. However, the excessively high surface energy of Cu(110) makes it susceptible to passivation *via* side reactions, thereby diminishing its lithiophilicity. Considering the overall balance of properties, Cu(100) emerges as the most promising orientation due to its optimal lattice matching and moderate surface energy (Fig. 3e).

However, it should be noted that the current mainstream methods for preparing single-crystal copper foils are still CVD and high-temperature degradation. For anode-free lithium metal batteries, these methods can neither meet the require-

Table 1 Principles and properties of the modified strategies

Scale	Strategies	Mechanism	Overpotential	CE (1st)	Dendrite	Stabilization
Atomic/nano	Crystal-facet engineering	Nucleation effect	Low	Medium	High	High
	Lithium-philic modification	Nucleation effect; influences SEI	Low	Medium	Medium	Medium
Micro-perspective	Artificial SEI	Regulation of Li flux; dense deposition	High	High	Low	High
	3D structural design	Regulation of Li flux; inhibition of expansion	High	Low	Low	High
Macro-perspective	Magnetic-field introduction	Regulation of Li flux	Medium	Low	Medium	High

 © 2026 The Author(s). Published by the Royal Society of Chemistry

Open Access Article. Published on 23 December 2025. Downloaded on 1/13/2026 8:44:30 PM.
This article is licensed under a Creative Commons Attribution-NonCommercial 3.0 Unported Licence.

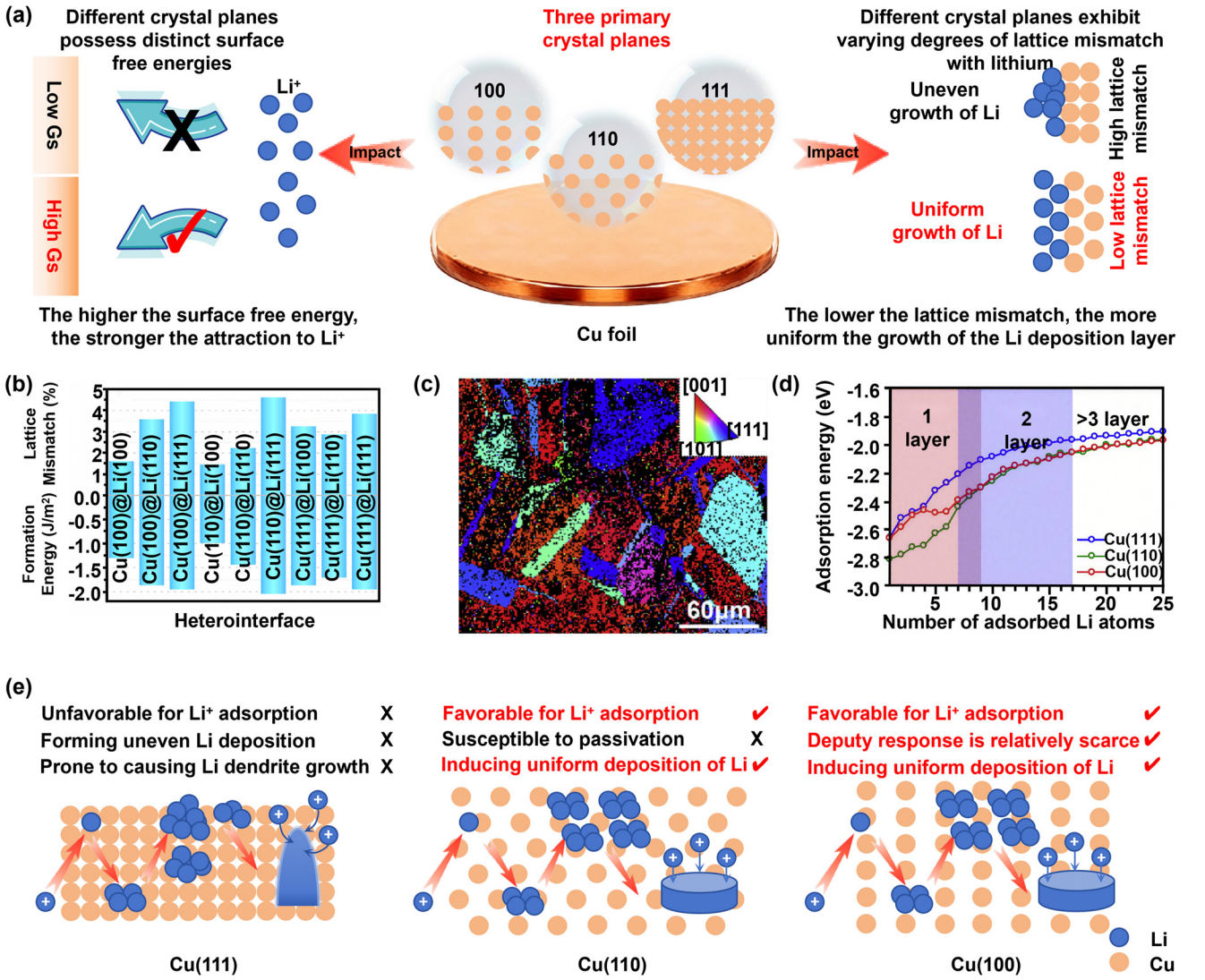

Fig. 3 (a) Schematic diagram of the characteristics of three crystal planes. (b) Lattice mismatches and binding energies of nine heterointerfaces per unit area.[44] Copyright © 2023, American Chemical Society. (c) Selective deposition of Li metal on the an-Cu current collector.[45] Copyright © 2019, Elsevier. (d) Adsorption energy of Li atoms on the Cu (111), (110) and (100) planes.[45] Copyright © 2019, Elsevier. (e) Schematic diagram of the effect of different crystal planes of copper foil on lithium deposition behavior.

ments of large-scale production nor reduce costs, making the facet control strategy difficult to implement. Developing single-crystal electroplating technology is an effective approach for achieving low-cost and large-scale production. The detailed parameters of the three production modes are listed in Table 2. In addition, for anode-free lithium metal batteries, electrodeposition provides a thickness-matched, crystallographically tailored, and manufacturing-compatible route that is inaccessible to both CVD and thermal recrystallization approaches. Electrodeposition uniquely enables direct fabrication of μm-thick single-crystal Cu foils under ambient conditions with high areal throughput and roll-to-roll compatibility, offering a collector-grade pathway intrinsically aligned with the manufacturing demands of anode-free lithium metal batteries. In contrast, CVD is fundamentally limited to thin-film regimes and serves primarily as a model platform, while high-temperature annealing suffers from stochastic grain evolution and low effective single-crystal yield.

2.2. Enhancing surface lithiophilicity

Beyond crystallographic tuning, introducing lithiophilic sites on the collector surface is an effective strategy to reduce the lithium nucleation barrier.[49] "Lithiophilicity" describes the affinity of a material or surface for lithium atoms, ions, or metal. Stronger lithiophilicity implies more facile and stable interactions with lithium. Lithiophilic sites are generally categorized into metallic sites and compound-based sites.[50–52] Metallic sites operate through alloying reactions with lithium, while compound sites often leverage the electronegativity of anionic groups combined with cation replacement reactions to

Open Access Article. Published on 23 December 2025. Downloaded on 1/13/2026 8:44:30 PM.
This article is licensed under a Creative Commons Attribution-NonCommercial 3.0 Unported Licence.

Table 2 Comparison of different preparation processes of single crystal copper foil

Metric	Electrodeposition	CVD	High-T annealing
Processing environment	Ambient pressure, wet process	High vacuum, gas-phase	High temperature, controlled atmosphere
Typical temperature	RT to 80 °C	700–1000 °C	900–1050 °C
Thickness suitability (10 μm)	Directly accessible	Fundamentally inefficient	Dependent on starting foil
Single-crystal scalability	Large-area, continuous	Limited by chamber size	Stochastic, non-uniform
Production mode	Roll-to-roll/continuous	Batch	Batch
Areal throughput	μm min^{-1}	nm to sub-μm min^{-1}	Hours per batch
Post-treatment process	No/optional mild annealing	Mandatory annealing	Mandatory annealing
Unit cost (10 μm)	6000–10 000 CNY m^{-2} (prediction)	≥30 000 CNY m^{-2}	15 000–30 000 CNY m^{-2}
Substrate transfer	Not required	Often required	Not required
Compatibility with battery manufacturing	High	Low	Medium
Relevance to anode-free LMBs	Intrinsic collector-grade foil	Model system only	Limited by grain boundaries
Overall industrial viability	**High**	**Low**	**Medium–low**

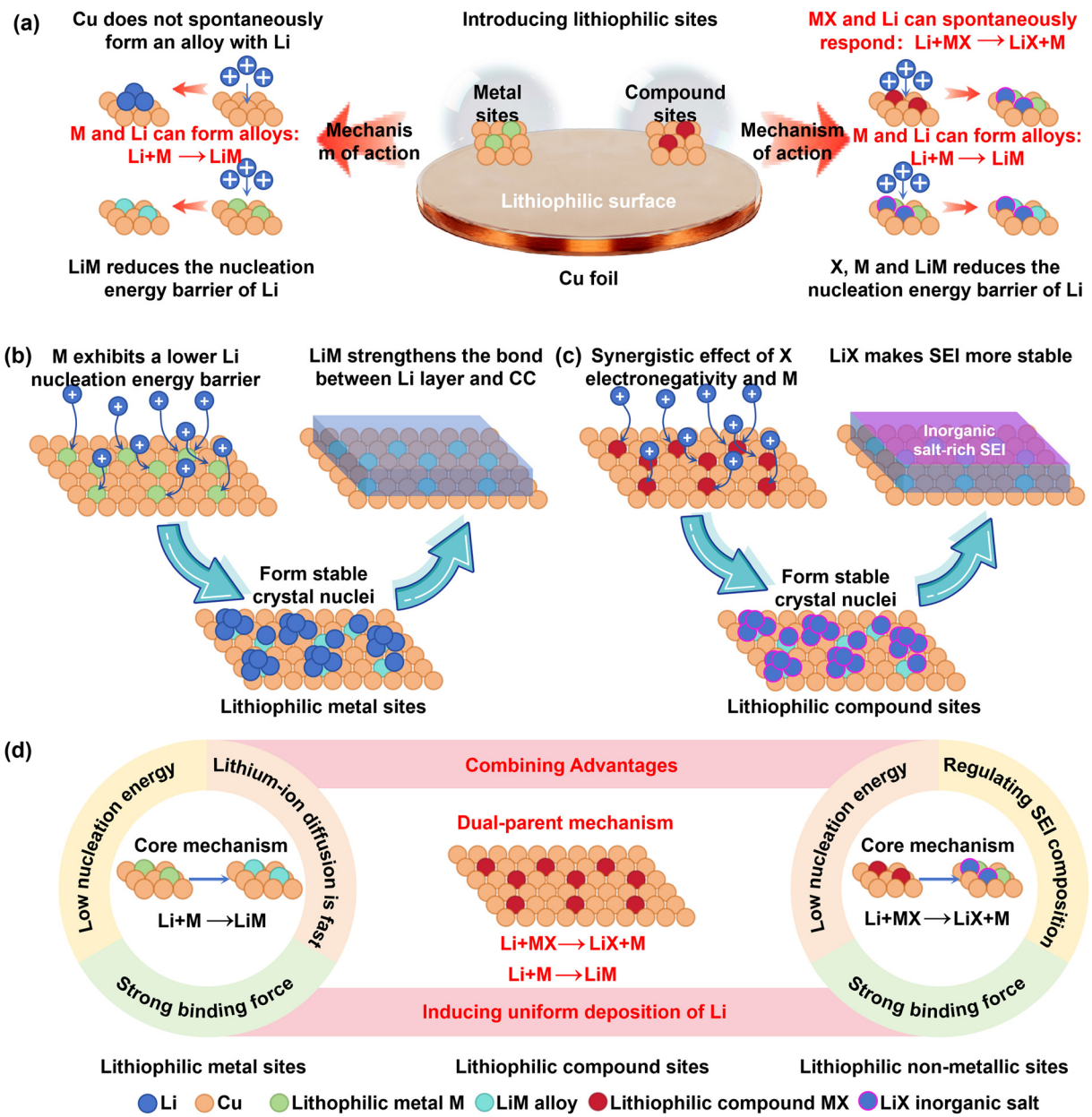

Fig. 4 (a) Schematic diagram of the lithiophilic mechanisms at two types of sites. Schematic diagram of (b) the influence of lithiophilic metal sites and (c) lithiophilic compound sites on lithium deposition behavior. (d) Characteristics of various lithium-affinity mechanisms.

 © 2026 The Author(s). Published by the Royal Society of Chemistry

Open Access Article. Published on 23 December 2025. Downloaded on 1/13/2026 8:44:30 PM.
This article is licensed under a Creative Commons Attribution-NonCommercial 3.0 Unported Licence.

direct lithium deposition, thereby extending cycling life (Fig. 4a).

2.2.1. Introducing lithiophilic metals. The lithiophilicity of metals primarily stems from their tendency to form alloys with lithium ($\Delta G < 0$), producing stable solid solutions or intermetallic compounds (*e.g.*, Li–Sn, Li–Zn, Li–Mg).[53–56] This alloying process, which involves lithium atoms being incorporated into the metal lattice, is spontaneous and reflects a high intrinsic affinity.[57] Techniques such as magnetron sputtering, melting, or electrodeposition can introduce these metals (*e.g.*, Au, Ag, Zn, Sn) onto Cu surfaces or form alloys (*e.g.*, Cu–Zn, Cu–Ga), thereby modifying the surface microstructure, affinity, and adhesion to regulate lithium deposition (Fig. 4b).[58–61]

During initial lithium deposition, the nucleation overpotential correlates with the solubility and lithiophilicity of the metal substrate. Metals like Au, Ag, Zn, and Mg, which exhibit significant solubility in lithium, can achieve near-zero nucleation overpotentials upon full lithiation. In contrast, metals with lower solubility, such as Al and Pt, show small but measurable overpotentials (5 mV and 8 mV, respectively).[53] Introducing lithiophilic metals not only lowers the nucleation barrier, facilitating the formation of stable nuclei, but also helps homogenize the Li^+ flux, preventing localized aggregation.[7] For instance, decorating copper foil with Ag nanoparticles, a $Cu_{0.64}Zn_{0.36}$ alloy layer, or a Sn layer significantly reduces the nucleation overpotential. Deposition preferentially occurs at these lithiophilic sites, promoting uniform Li^+ flux distribution. Notably, Sn(111) can induce the oriented growth of lithium along specific crystallographic directions (Li_7Sn_2(021) and $Li_{22}Sn_5$(822)), further enhancing deposition uniformity.[58,60–63]

Beyond nucleation, lithiophilic modifiers influence the subsequent growth stage by altering the dimensionality and migration rate of Li^+ diffusion on the collector surface.[64] For example, coating copper with liquid metal Ga forms an *in situ* $CuGa_2$ alloy layer that anchors the Ga. This modification reduces the lateral diffusion resistance for lithium, favoring two-dimensional planar deposition over dendritic growth, thereby improving the quality and stability of the lithium layer.[60]

Strong adhesion between the lithium deposit and the collector is crucial for performance stability. Insufficient adhesion can lead to detachment during repeated cycling, generating "dead Li" and capacity fade.[65–67] Thin layers of metals like Au, Ag, or Pt enhance adhesion by forming intermetallic compounds or solid solutions with lithium. This improved mechanical integrity helps maintain deposit stability even under high current densities and prolonged cycling.[62,68,69] It is noteworthy, however, that Au and Ag can exhibit excessive diffusion into lithium over time, gradually reducing surface lithiophilicity. In contrast, Pt, with its lower solubility, maintains more consistent lithiophilic properties. In addition, Zn, Sn and other metals have good solubility in Cu, and the high stability of this alloy state (solid solution) can make such lithium-philic metals exist stably on the surface of the collector, thus ensuring the long-term stability of the lithiumphilicity.[59,70] Furthermore, despite their high cost, ultrathin Au and Ag layers are still used in specific research contexts due to their excellent lithiophilicity and well-defined interfacial energetics. They are particularly useful when highly uniform nucleation or isolation of intrinsic deposition mechanisms is required, such as in pilot-scale demonstrations, extreme fast-charging (XFC) performance evaluations, and model interfacial studies. In practical scenarios demanding cost-effective implementation, low-cost lithiophilic materials (*e.g.*, Sn-based, Zn-based, and Ga-based coatings) serve as scalable alternatives. These materials reduce nucleation barriers through alloying or interfacial substitution reactions; however, compared with noble metals, they involve different trade-offs in mechanical and electrochemical properties.

In essence, leveraging alloying reactions enhances affinity, lowers nucleation barriers, and promotes stable nucleus formation. These modifications alter surface properties (roughness, adhesion), enrich active sites, and homogenize Li^+ distribution. Furthermore, the formation of solid solutions (atomic diffusion) or intermetallic phases (chemical bonding) strengthens the metallurgical bond between the lithium layer and the copper collector, mitigating detachment and ensuring cycling stability.[71–74]

2.2.2. Introducing lithiophilic compounds. Unlike metallic elements, the lithiophilicity of non-metals (*e.g.*, F, Cl, O) originates from their high electronegativity and ability to form strong chemical bonds with Li (*e.g.*, Li–F, Li–O), effectively reducing the nucleation barrier.[75–79] Furthermore, the resulting lithium-containing compounds (*e.g.*, LiF, Li_2O) are key components of high-quality SEI layers. These Li-rich inorganic salts typically facilitate high Li^+ flux and possess superior mechanical stability (Fig. 4c).[80–85]

Copper surfaces can be directly functionalized with these elements *via* etching or thermal treatment.[86–88] For example, selective etching creates a textured surface where formed CuCl structures act as "lithiophilic cages", significantly increasing the binding energy with Li and fostering a homogeneous, stable LiCl-rich SEI. This leads to uniform Li^+ flux and deposition, enabling an LFP||etch-Cu full cell to cycle stably for 500 hours (0.5C, CE ≈ 96%).[88] Alternatively, constructing an Ag@CuO heterostructure introduces oxygen.[77] During lithium deposition, a displacement reaction with CuO generates lithiophilic Li_2O, lowering the nucleation overpotential and promoting uniform nucleation. The *in situ* formed Li_2O-rich SEI further enhances Li^+ flux, guiding uniform deposition.

The displacement reaction strategy (Li + MX → M + LiX) can be extended by replacing the non-lithiophilic Cu with other lithiophilic metals.[89] These compounds significantly impact deposition behavior. Depositing a 50 nm ZnF_2 layer on copper, for instance, drastically reduces the nucleation overpotential from 79 mV to 11 mV (at 1 mA cm^{-2}), benefiting from the presence of lithiophilic Zn, LiF, and LiZn. This also increases the LiF content in the SEI, improving Li^+ flux and mechanical stability, enabling stable cycling even under high areal capacity (6 mAh cm^{-2}).[90]

Therefore, introducing lithiophilic metals addresses the high nucleation barrier on copper, promoting uniform deposition and extending battery life. Incorporating non-metallic

Open Access Article. Published on 23 December 2025. Downloaded on 1/13/2026 8:44:30 PM.
This article is licensed under a Creative Commons Attribution-NonCommercial 3.0 Unported Licence.

lithiophilic elements reduces the nucleation barrier by enhancing binding strength and modifying SEI composition. Compound-based lithiophilic modifiers, leveraging a dual-affinity mechanism, combine the advantages of both metallic and non-metallic elements, exerting the most profound influence on lithium deposition (Fig. 4d). In addition, surface lithiophilic modification may alter the interfacial double-layer structure and the surface state of the deposited lithium. Such changes could influence the adsorption and decomposition behavior of anions in the electrolyte, thereby modifying the composition and functionality of the resulting SEI. These interfacial effects require further investigation to deepen the mechanistic understanding of anode-free systems and to support the practical advancement of AFLMBs. Notably, the processes for introducing elements like Zn, Sn, or ZnF_2 are relatively straightforward and low cost, presenting promising prospects for industrial scaling and accelerating the practical application of lithium metal batteries.[72–77]

2.3. Constructing an artificial SEI (ASEI)

While surface lithiophilization effectively regulates lithium deposition in the nucleation and early growth stages, its efficacy can diminish at high currents (due to tip-enhanced dendrite growth) or with increasing deposit thickness (as lithium overburden covers the modified surface).[63] To address these limitations, research focus has expanded from the "foundation" (the substrate) to the "roof"—the SEI.

An ideal SEI should exhibit high Li^+ conductivity, excellent electrolyte wettability, robust physicochemical stability, and high mechanical strength.[91] Naturally formed SEIs, however, are often unstable, comprising irreversible and unstable electrolyte reduction products (*e.g.*, Li_2O, Li_2CO_3, $ROCO_2Li$, ROLi). Their continuous decomposition during cycling leads to side reactions, thick SEI formation, and electrolyte depletion, exacerbating active Li loss and inhomogeneous Li^+ flux, which in turn promotes dendrite growth and short circuits.[92]

Artificial solid electrolyte interphases (ASEIs) offer a "top-down" design strategy. By precisely controlling composition, ASEIs can isolate the lithium layer from the electrolyte, minimize parasitic reactions, and guide uniform lithium deposition—even under high current densities and capacities—acting like a protective "quilt" over the copper foil. As lithium deposits and accumulates, this "quilt" is pushed upward, remaining functional (Fig. 5a).[93]

ASEIs can be categorized into inorganic, organic, and composite types. Inorganic ASEIs, typically composed of lithiophilic inorganic materials (Li_3N, LiF, ZrO_2, Li_3Sb, Li_3Bi, *etc.*), offer extremely high Li^+ flux (supporting high-current cycling) and a high Young's modulus (resisting dendrite penetration) (Fig. 5b).[94] For instance, a dense, uniform inorganic ASEI comprising ZrO_2, Li_2O, Li_3N, and LiN_xO_y was formed *via* spontaneous reaction between lithium and a $ZrO(NO_3)_2$ solution. The abundance of grain boundaries in this multi-component ASEI facilitates rapid Li^+ diffusion, while its high modulus enables stable cycling for over 550 hours under demanding conditions (10 mA cm^{-2}, 10 mAh cm^{-2}).[95]

Hybridizing lithium salts with high modulus and lithium alloys with high diffusion coefficients can yield ASEIs with high ionic conductivity, electronic insulation, and thermodynamic stability. For example, a hybrid Li_3Sb/LiF ASEI leverages the ultra-high Li^+ diffusion coefficient of Li_3Sb (2.0×10^{-4} cm^2 s^{-1}) to eliminate diffusion barriers at high currents (up to 20 mA cm^{-2}), while LiF provides electronic insulation and mechanical strength.[96] Similarly, a Li_3Bi/LiF hybrid ASEI demonstrates high ionic conductivity (3.5×10^{-4} S cm^{-1}), high resistivity (9.04×10^4 Ω cm), and a high modulus (1348 GPa), ensuring uniform deposition at 20 mA cm^{-2}.[97] However, the high modulus of inorganic ASEIs often comes with brittleness. The significant volume changes during cycling can cause fracture, allowing electrolyte penetration and dendrite growth. Furthermore, their poor electrolyte wettability can lead to high interfacial polarization.[98,99]

Organic ASEIs are primarily based on polymer matrices functionalized with ion-conducting groups. These polymers offer good ionic conductivity, high flexibility (accommodating volume changes), and superior electrolyte wettability due to their functional groups (Fig. 5c).[100–102] For instance, incorporating porous xPCMS-g-PEGMA nanofillers into a lithiated single-ion conductive Nafion membrane enhances its mechanical strength *via* a hypercrosslinked core, while the PEGMA chains ensure homogeneous composite formation and facilitate efficient Li^+ transport. This ASEI enables a 2800-hour cycle life under 10 mA cm^{-2} and 10 mAh cm^{-2}.[103] Using a dynamic imine-based gel formed from flexible telechelic PEG and rigid chitosan also achieves a 3200-hour cycle life under similar conditions.[104] Drawbacks of organic ASEIs include generally lower mechanical strength (increasing dendrite penetration risk) and potential decomposition at high voltages.[105]

Composite ASEIs synergistically combine inorganic and organic components, aiming to achieve high ionic conductivity, thermodynamic stability, excellent wettability, dendrite suppression, and stress tolerance simultaneously (Fig. 5d).[106] One design features a multicomponent gradient ASEI with an outer layer of lithiated fluorinated carboxylate and an inner layer of LiF, Li_2S, and Li_2SO_3. This structure provides enhanced Li affinity and wettability, enables rapid Li^+ transport (supporting 15 mA cm^{-2}), suppresses dendrites, and ensures uniform deposition.[107] Another approach uses a LiBr-HBU layer, creating a uniform, dense hybrid ASEI with excellent electrolyte wettability/stability and high ionic conductivity (2.75×10^{-4} S cm^{-1}, ~50 times that of native SEIs). Symmetric cells with this modification show significantly improved performance, especially at high current densities (1333 hours at 15 mA cm^{-2}).[108]

Overall, the instability of native SEIs severely limits battery performance. ASEIs, through rational design and controlled composition, overcome these limitations, ensuring high ionic conduction, stability, and safety, making them a cornerstone technology for practical LMBs. Inorganic ASEIs excel in high-rate scenarios due to their high conductivity and modulus but suffer from brittleness. Organic ASEIs offer superior toughness for high-capacity cycling but face challenges in mechanical strength and voltage stability. Composite ASEIs merge these advantages, using organic phases to absorb stress and in-

 © 2026 The Author(s). Published by the Royal Society of Chemistry

Open Access Article. Published on 23 December 2025. Downloaded on 1/13/2026 8:44:30 PM.
This article is licensed under a Creative Commons Attribution-NonCommercial 3.0 Unported Licence.

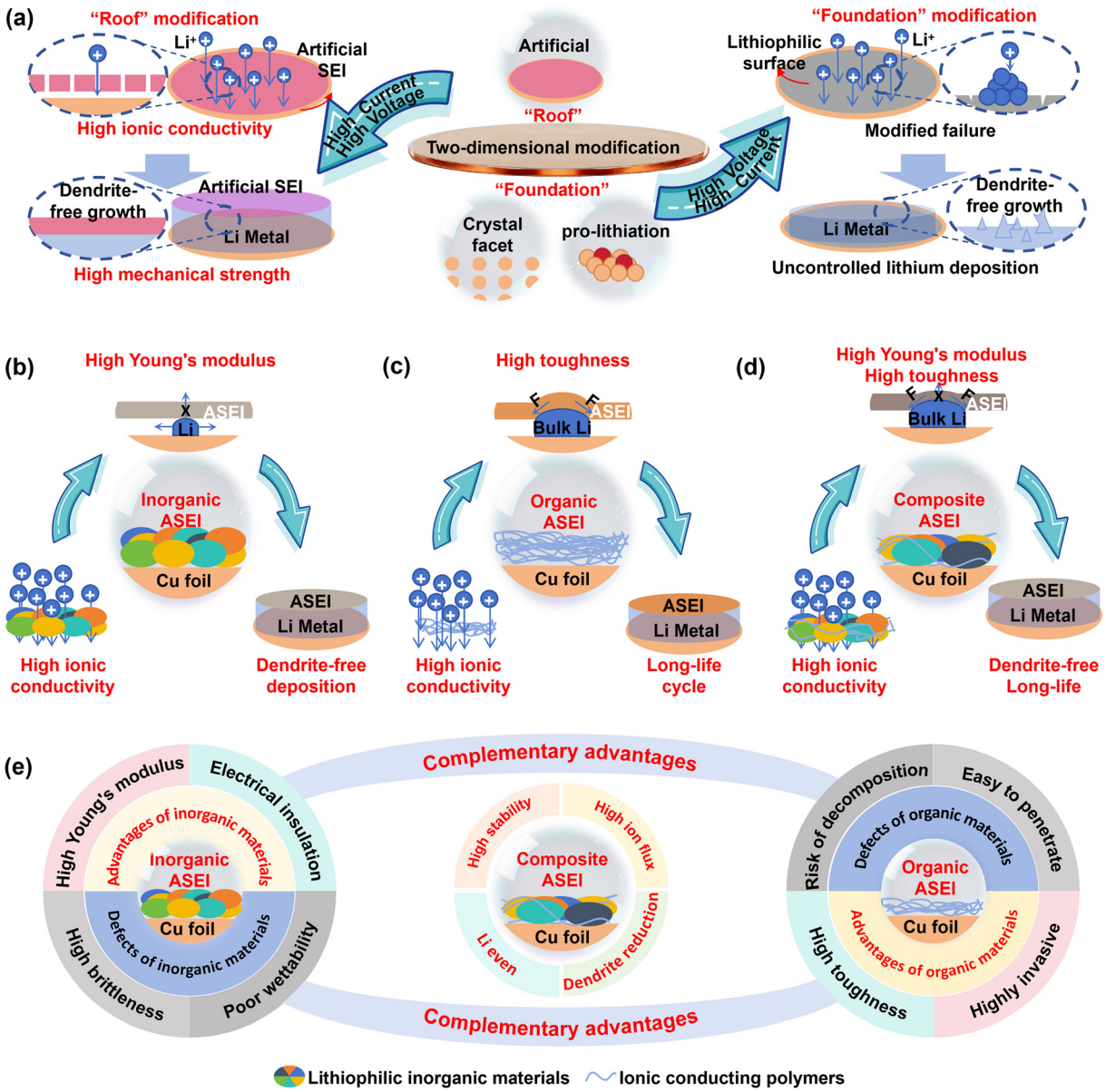

Fig. 5 (a) Schematic diagram of lithium deposition under high current and high capacity conditions using different modification methods. Schematic diagram of the effects of (b) inorganic ASEIs, (c) organic ASEIs, and (d) composite ASEIs on lithium deposition behavior. (e) Characteristics of each ASEI.

organic phases to provide strength and block decomposition pathways, ultimately delivering exceptional performance under both high-current and high-capacity conditions (Fig. 5e). Meanwhile, the ASEI can effectively suppress the occurrence of parasitic reactions by isolating the deposited lithium from direct contact with the electrolyte. Its high stability can mitigate corrosion-driven interfacial degradation and significantly reduce the risk of gas generation and explosion.

The path to widespread application, however, involves overcoming hurdles related to process complexity, scalability, and cost. Many current ASEI fabrication methods rely on sophisticated techniques like ALD or CVD, which are time-consuming and challenging to scale. Furthermore, the synergistic mechanisms within multi-component composite ASEIs require deeper understanding. Future efforts should focus on developing simple, low-cost manufacturing techniques and elucidating composition–structure–property relationships to accelerate the deployment of high-energy-density lithium metal batteries.[109]

3. Three-dimensional architecture design

While 2D copper current collector modifications effectively regulate lithium deposition under moderate conditions, their efficacy diminishes under high current densities or thick

Open Access Article. Published on 23 December 2025. Downloaded on 1/13/2026 8:44:30 PM.
This article is licensed under a Creative Commons Attribution-NonCommercial 3.0 Unported Licence.

lithium plating. This limitation arises from the dynamic shift in the deposition interface—from the electrolyte–collector boundary to an electrolyte–lithium interface—which progressively attenuates the surface modification effects. Concurrently, substantial volumetric expansion and accumulated mechanical stress can induce structural failure.[110] Under high current operation, the disparity in activity across surface sites is amplified, triggering heterogeneous lithium deposition and accelerating dendrite formation.[111]

In contrast, rationally designed 3D copper architectures present a paradigm shift. Their high specific surface area provides abundant nucleation sites while enabling more homogeneous electric field distribution and Li^+ flux redistribution, collectively guiding uniform, dendrite-free lithium deposition.[112] Current 3D Cu CC designs are primarily categorized into scaffold structures, porous frameworks, and gradient architectures.

3.1. Scaffold-structured frameworks

3D scaffolds typically consist of nano/microscale fibrous networks integrated onto a 2D copper foil substrate (Fig. 6a).[113] For instance, the etching and subsequent reduction of copper foil creates a submicron scaffold with nanoscale protrusions. This design significantly increases the specific surface area to disperse local current density, provides efficient electron conduction pathways, and ensures structural stability. The protruding tips on each fiber act as active nucleation sites, promoting uniform electric field distribution for dendrite-free deposition.[114] Alternatively, a one-step coelectrodeposition method can fabricate a 3D copper-based scaffold by depositing carbon nanotubes (CNTs) and copper simultaneously onto a foil. The uniform copper coating on CNTs prevents excessive exposed carbon that could trigger additional SEI formation. After calendaring to optimize density, the Li‖3D Cu/CNT half-cell maintains a high coulombic efficiency of 99% over 800 cycles.[115]

Despite these improvements, the intrinsic lithiophobicity of copper ultimately limits the performance ceiling of 3D scaffolds. Integrating lithiophilic modifications has thus become a crucial strategy for enhancing their electrochemical performance (Fig. 6b).[116] For example, magnetron sputtering was used to selectively decorate copper fibers with lithiophilic tin sites or an

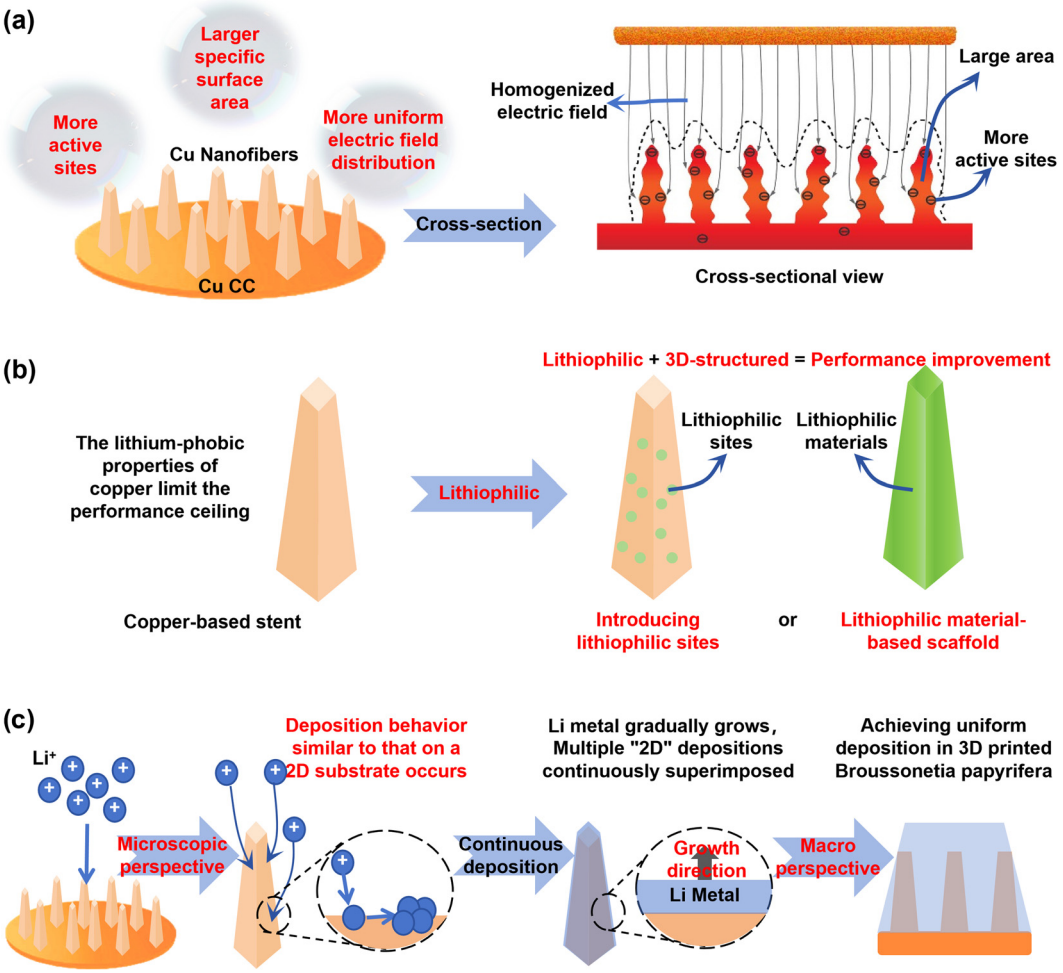

Fig. 6 (a) Schematic diagrams of 3D scaffold structures, along with its cross-sectional view. Copyright © 2015, C. Yang *et al.*[114] (b) Schematic diagram of lithiophilic scaffold construction. (c) Schematic diagram of uniform Li deposition induced by scaffold structure.

 © 2026 The Author(s). Published by the Royal Society of Chemistry

Open Access Article. Published on 23 December 2025. Downloaded on 1/13/2026 8:44:30 PM.
This article is licensed under a Creative Commons Attribution-NonCommercial 3.0 Unported Licence.

ultrathin zinc oxide layer. By enhancing electron conduction and Li^+ diffusion rates, these modifications successfully guided uniform lithium deposition. The 3D scaffold's high surface area and reduced local current density, combined with uniformly distributed tin sites, created a rapid electron-ion transport network. This synergy enabled a symmetric cell with the Sn–Cu collector to achieve an extended cycle life of nearly 1500 hours at 3 mA cm^{-2} and 6 mAh cm^{-2}.[59] Similarly, a copper scaffold coated with an ultrathin Zn layer demonstrated exceptional stability in symmetric cells (4 mA cm^{-2}, 500 h) and full cells (81% capacity retention after 1000 cycles).[117]

Beyond metallic coatings, scaffolds incorporating lithiophilic metals, carbon-based materials, and metal–organic frameworks (MOFs) have been widely explored.[118–121] One design features a 3D Cu/CNT/Sn composite collector with a tin-coated CNT scaffold on copper foil.[120] Another innovative approach synthesized a Co@Zn-CNT scaffold grown *in situ* on cobalt centers, with atomically dispersed zinc species on the outer sheath.[121] The CNT matrix enhances structural stability, while the Sn layer or Zn species serve as lithiophilic sites to guide uniform Li deposition. The modified Co@Zn-CNT-Cu electrode enables dense, uniform lithium deposition even at high areal capacities (10 mAh cm^{-2}) while maintaining excellent cycling stability and capacity retention.

In essence, the nanofibrous network partitions the lithium deposition process into numerous independent microdomains (Fig. 6c). Within each domain, deposition occurs on a stable fibrous substrate, mimicking the homogeneous mechanism on 2D foil. This structural segmentation achieves uniform electric field distribution, promotes homogeneous Li^+ flux, suppresses dendrite growth, and ultimately induces uniform lithium deposition across the entire electrode.

3.2. Porous framework designs

Porous structures offer an even higher specific surface area than scaffolds, providing more active sites and more uniform electric field distribution.[122] Their interconnected pore channels ensure efficient Li^+ diffusion, further inhibiting dendrite growth.[123,124] Unlike scaffolds that provide deposition guides, porous skeletons partition space into interconnected compartments. Li^+ initially deposits onto the skeleton, and these compartments are gradually filled during plating, eventually forming a uniform lithium coating that encapsulates the structure (Fig. 7a).

For instance, electrochemical dealloying of zinc from brass produces a 3D porous copper structure with an average thickness of ~14 μm and ~72% porosity. This collector effectively suppresses lithium dendrite growth even at high areal capacities (10 mAh cm^{-2}) and current densities (10 mA cm^{-2}).[125] Alternatively, electrodeposited 3D interconnected copper foam with a "lithium dendrite cage" structure utilizes its internal pores to accommodate dendrites, inhibiting vertical growth and mitigating volume changes.[126]

Introducing lithiophilic sites remains an effective strategy to overcome copper's inherent lithiophobicity in 3D porous frameworks. Researchers have loaded Cu_2Se/Cu_2O heterostructured nanowires as kinetically enhanced nucleation sites. Leveraging the synergy between optimized pore structure and heterostructured nanowires, the Cu_2Se/Cu_2O@3D Cu compo-

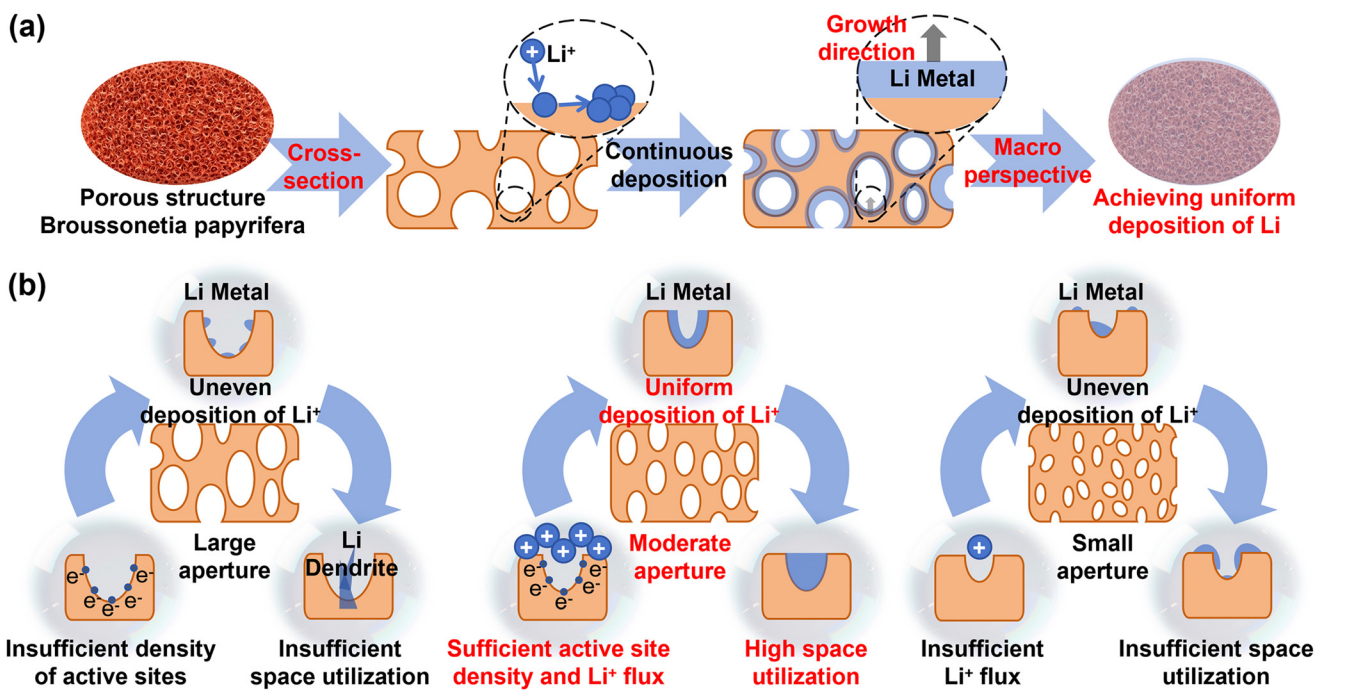

Fig. 7 (a) Schematic diagram of uniform Li deposition induced by porous structure. (b) Schematic diagram of the effect of pore size on Li deposition.

Open Access Article. Published on 23 December 2025. Downloaded on 1/13/2026 8:44:30 PM.
This article is licensed under a Creative Commons Attribution-NonCommercial 3.0 Unported Licence.

site collector exhibits exceptional dendrite-suppression capability and electrochemical performance: an ultra-long symmetric cell lifespan of 3000 hours at 1 mA cm^{-2}, remaining stable for 300 h even at 20 mA cm^{-2}.[127]

Pore size critically influences deposition behavior (Fig. 7b). Excessively large pores reduce active site density, while overly small pores impede Li^+ diffusion.[127] Commercial copper foam, with its large pore sizes (150–400 μm), often suffers from insufficient conductive contact and physical support within the pores, reducing deposition/stripping reversibility and inevitably leading to dendrites and failure.[128] Using the hydrogen bubble template (HBT) method, Guo *et al.* prepared a series of 3D porous copper collectors with varying pore sizes and wall structures. The best performance was achieved with a 3D Cu structure featuring an average surface pore size of 25.18 μm and the lowest distribution probability (32.08%) of macropores (100–250 nm) in the pore walls.[127]

3.3. Gradient architectures

The performance gains from scaffold and porous designs confirm that 3D structures effectively regulate internal electric fields and Li^+ flux.[129,130] However, in practical application, homogenous 3D frameworks like standard copper foam suffer from current concentration effects. Lithium preferentially nucleates and grows on the top surface, progressively blocking the structure and hindering Li^+ transport to the interior, thus underutilizing the 3D framework (Fig. 8a).[131]

Constructing gradient structures by introducing varying lithiophilic properties from the interior to the surface can significantly improve spatial utilization and promote denser lithium deposition (Fig. 8b).[132,133] As established, the Cu(100) facet exhibits superior lithiophilicity compared to Cu(111). Leveraging this difference, a gradient structure can be created. For instance, inducing a preferential Cu(100) orientation at the bottom and a Cu(111) orientation at the top of a wavy or grooved copper collector forms a lithiophilicity gradient. This design promotes preferential deposition at the bottom, alleviating current concentration at the top, homogenizing the electric field, suppressing dendrites, and directing more Li^+ to deposit internally, thereby enhancing spatial utilization efficiency. A wavy copper substrate with a high, gradient Cu (100) texture (ranging from 96.80% in the valleys to 47.10% on the peaks) used as a current collector in AFLMBs demonstrated remarkable capacity retentions of 87% (120 cycles) with $LiFePO_4$ and 77% (110 cycles) with $LiNi_{0.8}Co_{0.1}Mn_{0.1}O_2$ cathodes. This design successfully achieved the preferential deposition of Li at the bottom.[134,135] Beyond crystallographic control, a dual-gradient structure was created by doctor-blading a liquid metal (GaInSn) layer onto copper foam as a gradient lithiophilic layer and depositing a nanoscale gold layer at the bottom as a conductive gradient. This design endowed the electrode with exceptional cycling performance: a half-cell lifespan exceeding 850 hours (5 mAh cm^{-2}), a high pore utilization rate of 88.80%, and no dendrite formation. The corresponding full cell with $LiFePO_4$ cathode sustained over 2000 cycles with 80% capacity retention at 1C.[136]

In conclusion, 3D current collector design demonstrates significant advantages in reducing local current density and promoting uniform lithium deposition, establishing itself as a potent strategy for optimizing lithium metal anodes. However, a critical consideration for their application in AFLMBs—which lack supplemental active lithium—is their high surface

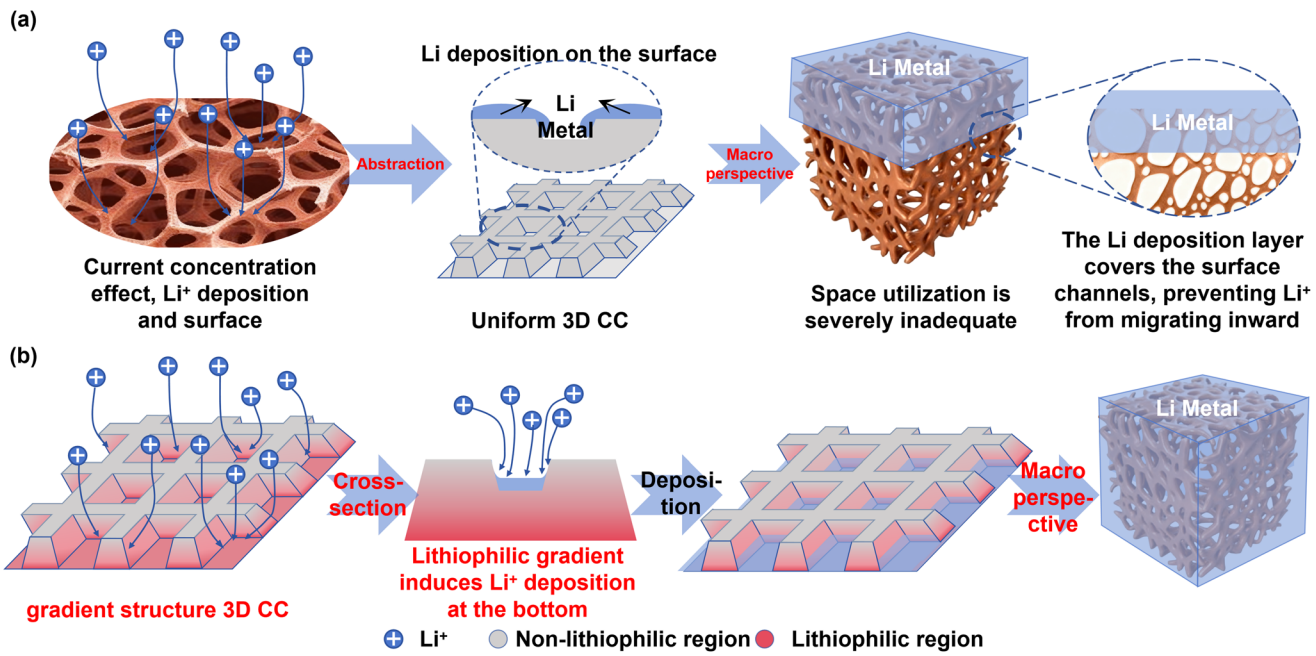

Fig. 8 (a) Schematic diagram of the effect of current concentration on Li deposition behavior. (b) Schematic diagram of the effect of 3D gradient structure on Li deposition behavior.

 © 2026 The Author(s). Published by the Royal Society of Chemistry

Open Access Article. Published on 23 December 2025. Downloaded on 1/13/2026 8:44:30 PM.
This article is licensed under a Creative Commons Attribution-NonCommercial 3.0 Unported Licence.

area, which necessitates extensive SEI formation. The continuous reformation and fracture of the SEI during cycling can drastically accelerate the irreversible consumption of the limited lithium inventory, severely limiting the cycle life of AFLMBs.[137] Consequently, research on 3D copper current collectors for AFLMBs remains at a nascent but highly promising stage of exploration.

4. Magnetic field-enhanced current collectors

In industrial electroplating, magnetic fields have long been employed to refine grain structure, control texture, and direct dendrite growth in metal deposits.[138,139] This approach leverages the magnetohydrodynamic (MHD) effect, where Lorentz forces act on conductive fluids (*e.g.*, liquid metals, electrolytes) in a magnetic field, inducing convective flows that enhance mass transport and homogenize ion distribution (Fig. 9a). Inspired by this mature technology, introducing magnetic fields to regulate lithium deposition has emerged as a highly effective strategy.[140–143] During battery operation, the steady migration of Li^+ to the negative electrode resembles a micro-scale electroplating process.[144,145] Under a sole electric field, inherent field inhomogeneities cause uneven Li^+ concentration at the collector surface, accelerating dendritic growth. The incorporation of a magnetic field uniformly generates multiple MHD micro-vortices within the cell. This micro-circulation of the anode-side electrolyte enhances mass transport, homogenizes the Li^+ concentration at the interface, and ultimately promotes uniform lithium deposition (Fig. 9b).[146–148]

Magnetic field application is typically categorized into external and internal configurations. Applying an external magnetic field to the lithium metal anode, for instance, subjects Li^+ to Lorentz forces during electrodeposition, inducing helical motion and activating the MHD effect. This results in markedly more uniform lithium deposition (Fig. 9c), significantly improving cycling lifespan and coulombic efficiency.[148] However, external fields, often generated by electromagnets, can lead to bulky, heavy battery systems. Furthermore, in practical applications, external magnetic fields may cause electro-

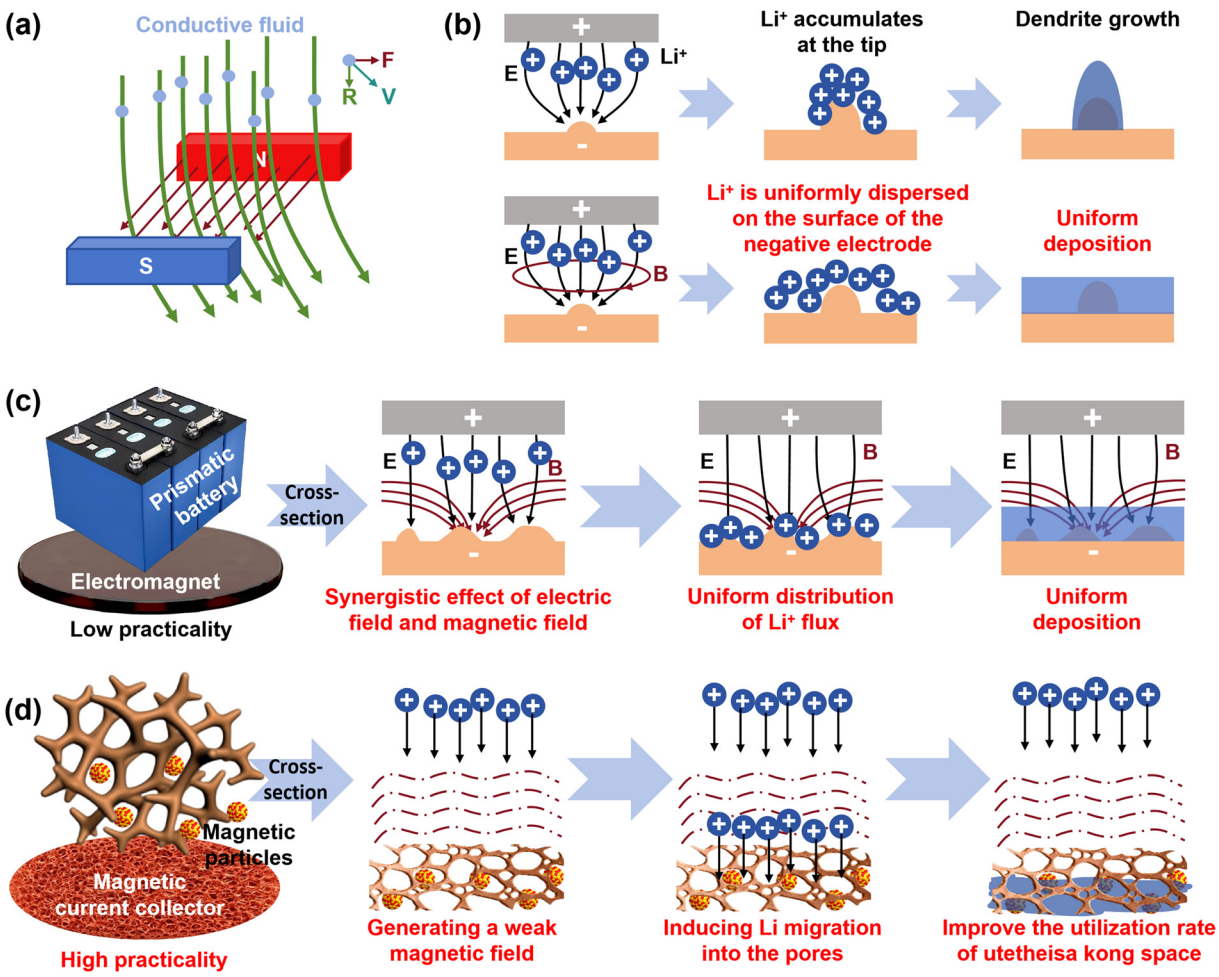

Fig. 9 (a) Schematic diagrams of magnetohydrodynamics. (b) Schematic diagram of the inductive effect of magnetic field on lithium ions. (c) Introduction of external magnetic field and its mechanism of action. (d) Construction of the magnetic current collector and its mechanism of action.

Open Access Article. Published on 23 December 2025. Downloaded on 1/13/2026 8:44:30 PM.
This article is licensed under a Creative Commons Attribution-NonCommercial 3.0 Unported Licence.

magnetic interference, disrupting the operation of sensitive integrated electronics.[149]

To circumvent these issues, research has shifted focus to internally generated magnetic fields by decorating copper current collectors with magnetic materials, particularly ferromagnetic substances.[150] Constructing a magnetic copper collector not only leverages the MHD effect for uniform plating but also addresses the challenge of insufficient spatial utilization in 3D frameworks (Fig. 9d).[151,152] For example, a magnetic collector was designed by growing MOF-74(Ni) on a copper foam (CF) substrate.[153] The introduced high-porosity magnetic MOF-74 effectively reduced local current density, provided abundant nucleation sites, and significantly enhanced Li^+ mobility at the collector surface. This synergy suppressed dendrite growth, fostered a stable SEI, and enabled deep lithium deposition, with Li^+ mobility increasing approximately sixfold compared to a non-magnetic environment.

Further enhancing this concept, Sheikholeslami *et al.* reported that smaller ferromagnetic particles (*e.g.*, Fe–Co–Ni alloys) generate stronger driving forces under an applied field.[154] The superimposed effect of the magnetic field and ferromagnetic particles can more effectively accelerate Li^+ migration, facilitating dense lithium deposition deep within the CF scaffold. Building on this, a 3D copper-based magnetic and lithiophilic collector (CNZ) was constructed by integrating a Ni–Co alloy (internal micro-magnet) with ZnO (lithiophilic sites).[155] The micro-magnetic field generated by the alloy boosted the depth of lithium deposition from 300 μm in plain CF to 1000 μm, while the ZnO sites reduced the nucleation overpotential, enabling a uniform and dense lithium metal layer.

Notably, in lithium–sulfur (Li–S) batteries, magnetic current collectors exert positive effects on both electrodes. Beyond the anode-side MHD effect, the magnetic catalytic effect (MCE) allows for tailoring the catalytic properties of ferromagnetic materials by modulating their electronic structure.[156,157] For instance, a magnetic field can trigger a spin-state transition in Co atoms of a ferromagnetic CoS_x catalyst from low-spin to high-spin, generating unpaired 3d electrons and lowering the free energy barrier for lithium polysulfide (LiPS) redox reactions.[158] Moreover, under a magnetic field, unconventional d–p hybridized ferromagnetic Fe_3M (M = Al, Si, Ga, Ge, Sn) materials exhibit significantly enhanced d–p hybridization near the Fermi level due to increased electron cloud overlap between M and Fe atoms, substantially boosting the overall kinetics of the Li–S reaction system.[159] These findings demonstrate that magnetic collectors can holistically improve Li–S battery performance and provide a promising development pathway for future designs.

In conclusion, existing studies generally suggest that the introduction of internal magnetic fields can trigger MHD convection in the electrolyte, which effectively homogenizes lithium-ion flux near the electrode surface. As a result, lithium deposition under magnetic-field-assisted conditions tends to be more spatially uniform, with suppressed concentration gradients and the formation of relatively dense and compact lithium layers compared with magnet-free systems.[147] Nevertheless, current evidence regarding the role of magnetic fields in preferential lithium deposition remains limited. Reports that directly correlate magnetic-field-induced ion transport with facet-selective growth, orientation preference, or intrinsic crystallization pathways of lithium are still scarce. The lack of systematic experimental data and quantitative analysis makes it challenging to decouple transport-driven effects from intrinsic deposition kinetics, thereby hindering the development of accurate and predictive theoretical models that describe magnetic-field-mediated lithium deposition. Addressing this knowledge gap will require coordinated experimental design and modeling efforts in future studies.

In addition, it is worth noting that despite the promising role of magnetic-field-assisted strategies in regulating lithium-ion flux and deposition behavior, it should be emphasized that current studies remain largely confined to coin-cell or symmetric-cell configurations. Existing experiments primarily focus on demonstrating the feasibility of magnetohydrodynamic (MHD)-induced convection in suppressing concentration polarization and regulating initial lithium nucleation at small scales. To date, there are no systematic reports on the implementation of embedded magnetic structures in stacked pouch-cell configurations, and consequently, quantitative evaluation of flux uniformity and long-term structural stability at the device-relevant scale remains elusive.

From a practical perspective, extending magnetic-field-assisted designs to stacked pouch cells introduces several unresolved challenges, including maintaining uniform magnetic field distribution across multilayer electrodes, ensuring sufficient penetration depth and the effectiveness of magnetic structures in thick electrodes, and understanding the coupled evolution of magnetic functionality and electrochemical stability during prolonged cycling. Addressing these issues will be essential for translating magnetically modulated lithium deposition from proof-of-concept demonstrations toward realistic anode-free lithium metal battery systems.

5. Summary and prospective

Lithium metal batteries represent a pivotal direction for next-generation high-energy-density storage, with the core challenge lying in controlling lithium deposition behavior on copper current collectors. This review has systematically examined modification strategies—spanning 2D surface engineering, 3D architectural design, and magnetic field regulation—demonstrating how optimized nucleation kinetics, suppressed dendrite growth, and stabilized SEI layers significantly enhance cycling stability and safety (summarizing the representative modification systems and their key electrochemical parameters in recent studies in Table 3). Despite remarkable progress, bridging the gap from laboratory prototypes to commercial deployment requires multi-faceted bottlenecks to be overcome, necessitating coordinated advances in theoretical understanding, material design, and engineering integration. Key challenges and future directions are outlined below.

 © 2026 The Author(s). Published by the Royal Society of Chemistry

Open Access Article. Published on 23 December 2025. Downloaded on 1/13/2026 8:44:30 PM.
This article is licensed under a Creative Commons Attribution-NonCommercial 3.0 Unported Licence.

Table 3 Summary of the current modification strategies

Anode	Half-cell parameters	CE (%)	Cycle number	Full-cell parameters	Cathode	Energy density	Initial CE (%)	Cycle number	Capacity retention	E/C	N/P	Electrolyte volume	Temp.	Ref.
An-Cu	1 mA cm^{-2} 1 mAh cm^{-2}	97.7	60	1C	LFP	—	—	240	57.1%	—	—	100 μL	Room temp.	45
CuCC-SSIC	0.5 mA cm^{-2} 1 mAh cm^{-2}	99.4	400	0.2C/0.3C	NCM811	350 Wh kg^{-1}	~60.0	100	54.8%	—	—	—	Room temp.	47
Cu| Ag@PDA-GO	0.2 mA cm^{-2} 1.6 mAh cm^{-2}	98.1	45	0.5 mA cm^{-2}	NCM111	—	86.3	80	65.5%	—	—	50 μL	Room temp.	63
Etch-Cu	0.5 mA cm^{-2} 0.5 mAh cm^{-2}	98.0	—	0.5C	LFP	—	~80.0	500	53.7%	—	—	—	Room temp.	88
LiF-LiZn/Cu	1 mA cm^{-2} 2 mAh cm^{-2}	99.2	200	1 mA cm^{-2}	NCM811	—	~99.0	50	88.0%	—	0.9	—	Room temp.	90
LiZrO $(NO_3)_2$@Cu	1 mA cm^{-2} 1 mAh cm^{-2}	96.2	100	0.5C	LCO	—	~90.0	100	72.4%	—	—	50 μL	Room temp.	95
LiF/Li_3Sb	—	—	—	3C	S	325.28 Wh kg	~100	60	91.5%	3 μl mg^{-1}	—	~1.3 mL	Room temp.	96
Li_3Bi/LiF	—	—	—	0.2C	NCM811	—	~81.0	100	79.2%	—	—	100 μL	Room temp.	97
xPCMS-g-PEGMA/LN	1 mA cm^{-2} 1 mAh cm^{-2}	99.2	300 h	0.5C	LFP	—	~97.0	100	79.0%	—	—	50 μL	Room temp.	103
DFFSA–Li	1 mA cm^{-2} 1 mAh cm^{-2}	99.0	65 h	0.2C/0.5C	NCM811	461.6 Wh kg^{-1}	~85.0	100	84.7%	1.6 g Ah^{-1}	1.28	8.78 g	Room temp.	107
3D Cu-CNT	0.5 mA cm^{-2} 1 mAh cm^{-2}	98.3	800	0.2C	LFP	—	—	20	73.0%	—	—	—	Room temp.	115
Zn/ZnO@Li	0.5 mA cm^{-2} 1 mAh cm^{-2}	98.0	160	2C	LTO	—	~95.0	1000	81.0%	—	—	60 μL	Room temp.	117
3D Cu	1 mA cm^{-2} 1 mAh cm^{-2}	96.0	100	1C	LFP	—	~80.0	100	82.6%	—	—	—	Room temp.	125
Cu_2Se/Cu_2O@3D Cu	1 mA cm^{-2} 1 mAh cm^{-2}	97.2	500	2C	LFP	—	~97.0	600	72.0%	—	—	50 μL	Room temp.	127
LHC600	1 mA cm^{-2} 1 mAh cm^{-2}	97.4	350	1C	LFP	—	~87.0	400	81.2%	—	2.79	40 μL	Room temp.	134
CNZ	1 mA cm^{-2} 1 mAh cm^{-2}	95.0	590	1C	LFP	—	~99.0	300	80.0%	—	—	—	Room temp.	155

Open Access Article. Published on 23 December 2025. Downloaded on 1/13/2026 8:44:30 PM.
This article is licensed under a Creative Commons Attribution-NonCommercial 3.0 Unported Licence.

5.1. Limitations of current modification strategies

While 2D surface engineering improves deposition uniformity through crystallographic tuning, lithiophilic modification, and artificial SEIs, its efficacy diminishes under high current densities or large areal capacities due to lithium overburden or SEI fracture. Alloy-based lithiophilic layers effectively reduce nucleation barriers, yet the high cost of noble metals (*e.g.*, Au, Ag) impedes scalable application. Artificial SEI layers often face trade-offs between chemical stability and mechanical strength, and complex fabrication routes (*e.g.*, CVD, electrospinning) hinder industrial adoption. 3D frameworks mitigate local current density *via* their high surface area but exacerbate active lithium consumption through continuous SEI formation/fracture, ultimately impairing cycle life. Magnetic field regulation homogenizes Li^+ distribution *via* MHD effects, yet external magnets introduce bulk and electromagnetic interference, while the long-term stability and field attenuation of embedded magnetic particles remain inadequately studied. Furthermore, compatibility between electrolytes and modified copper surfaces is often overlooked; certain lithiophilic layers may trigger side reactions, accelerating active lithium loss, which is a critical concern for anode-free configurations lacking lithium reserves.

5.2. Performance degradation in practical scenarios

Laboratory protocols, optimized for fundamental insight, typically employ low current densities (0.1–0.5 mA cm^{-2}) and excess lithium (*e.g.*, 5 mAh pre-plated Li cycling 1 mAh). These conditions diverge sharply from real-world operation. In electric vehicles and grid storage, fast-charging demands (2–5C) induce deposition rates exceeding Li^+ diffusion, leading to localized ion accumulation, dendritic growth, and internal short-circuit risks. Pre-plated lithium masks irreversible loss during initial SEI formation, inflates coulombic efficiency metrics, and reduces practical energy density. Moreover, small-format coin cells fail to replicate challenges in pouch cells—volume expansion, interfacial impedance accumulation, and rate capability decay are markedly exacerbated at larger scales. For instance, 3D copper structures may collapse under mechanical stress in pouch cells, and magnetic field uniformity becomes difficult to maintain in multi-layer stacks, collectively limiting energy density and cycle life.

In addition to performance enhancements, the practical implementation of copper current collector engineering for anode-free lithium metal batteries necessitates careful consideration of risk assessment and quality-control issues. In such systems, rigorous verification of complete lithium stripping is particularly critical, as residual inactive lithium or partial reversibility may lead to inaccurate coulombic efficiency while obscuring progressive degradation processes. Moreover, operation under practical conditions—such as high current densities and fast-charging protocols—introduces elevated safety risks that remain insufficiently addressed in most laboratory-scale studies.

From a broader perspective, the lack of standardized evaluation methodologies represents a key barrier to the rational comparison of different copper current collector designs. Performance metrics commonly reported in the literature, especially coulombic efficiency, are often insufficient to fully capture failure modes associated with non-uniform lithium

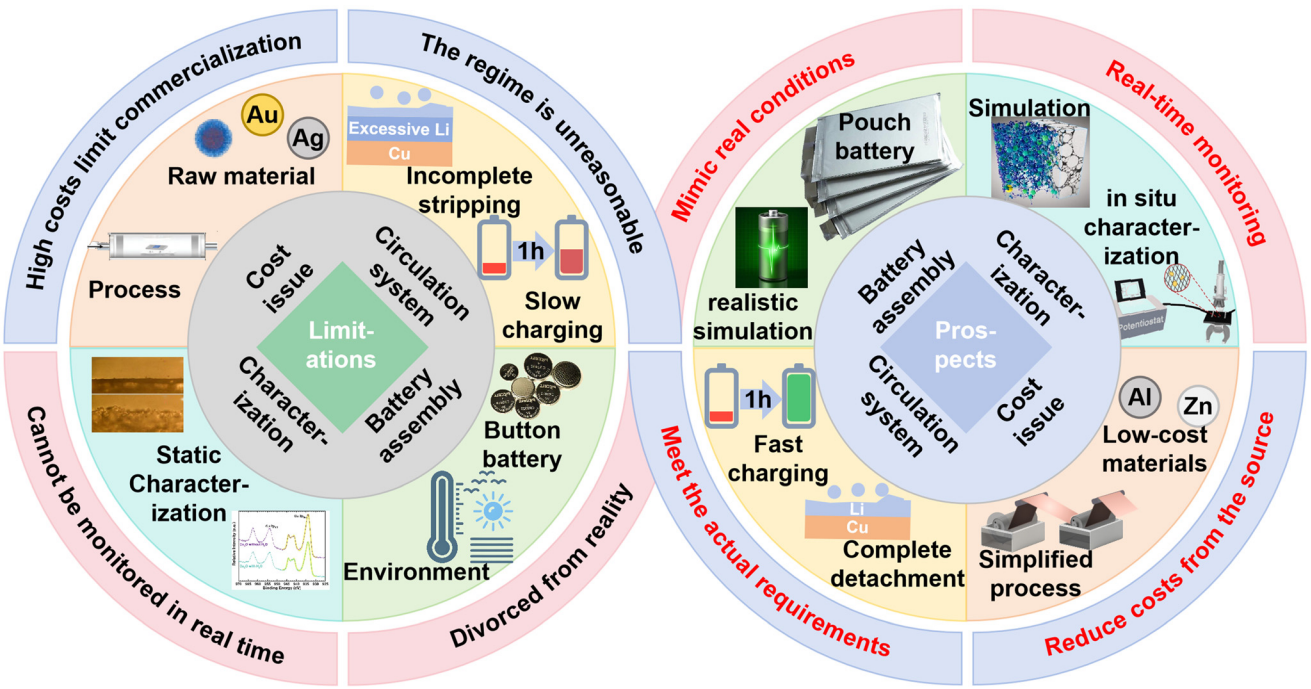

Fig. 10 Current issues and outlook for future development.

 © 2026 The Author(s). Published by the Royal Society of Chemistry

Open Access Article. Published on 23 December 2025. Downloaded on 1/13/2026 8:44:30 PM.
This article is licensed under a Creative Commons Attribution-NonCommercial 3.0 Unported Licence.

deposition, interfacial instability, or mechanical degradation. Therefore, future studies should emphasize the integration of *operando* and *in situ* diagnostic tools, including optical monitoring, stress or pressure analysis, and X-ray-based techniques, to enable more reliable assessment of reliability and reproducibility. Addressing these challenges will be essential for translating copper current collector design strategies from proof-of-concept demonstrations to practical anode-free battery systems (Fig. 10).

In summary, copper current collector modifications provide a cornerstone for practical high-energy-density batteries. The synergistic development of 2D surface, 3D structural, and magnetic strategies has markedly improved cycling stability and energy density. Future efforts must prioritize commercial viability. For example, single-crystal copper foils—currently produced *via* costly CVD processes—require low-cost, scalable alternatives like electroplating to enable large-format battery manufacturing. In anode-free LMBs, where no excess lithium compensates for irreversible loss, achieving high reversibility—especially during the first cycle where significant active lithium is consumed in SEI formation—is paramount. Enhancing first-cycle coulombic efficiency is a critical milestone for commercial viability.

Testing protocols must evolve to mirror real-world conditions: fast-charging capability should be emphasized, and discharge should ensure complete lithium stripping to maximize energy density. Current understanding of lithium deposition, largely derived from "static post-mortem analysis in coin cells", lacks insights into dynamic processes under practical operation. Advanced *in situ*/*operando* characterization techniques are essential to observe deposition/stripping behavior in real time, guiding precision engineering of interfaces.

Through deeper integration of fundamental research and scalable engineering, modified copper current collectors are poised to accelerate the adoption of lithium metal and anode-free batteries in electric vehicles and grid storage, injecting renewed momentum into the development of advanced energy storage technologies.

Author contributions

Jiawang Feng: conceptualization, investigation, writing – original draft, writing – review and editing, visualization; Tianzhengyi Zhang, Ming Liu, Guoxing Tian: conceptualization, investigation, writing – review and editing, supervision; Yuqian Fan, Ailing Song, Guangjie Shao, Zhipeng Ma: conceptualization, investigation, supervision.

Conflicts of interest

The authors declare no conflict of interest.

Data availability

Data sharing is not applicable to this article as no new data were created or analyzed in this study.

Acknowledgements

This work was financially supported by the National Natural Science Foundation of China (52074241, 52174281, 51674221 and 51704261), the Hebei Province Natural Science Foundation (B2025203050), the Science and Technology Project of Hebei Education Department (BJ2020038) and the Cultivation Project for Basic Research and Innovation of Yanshan University (2024LGQL003).

References

1 Y. Ding, Z. P. Cano, A. Yu, J. Lu and Z. Chen, *Electrochem. Energy Rev.*, 2019, **2**, 1–28.
2 S. Yuan, T. Kong, Y. Zhang, P. Dong, Y. Zhang, X. Dong, Y. Wang and Y. Xia, *Angew. Chem., Int. Ed.*, 2021, **60**, 25624–25638.
3 W. Ai, Z. Huang, L. Wu, Z. Du, C. Zou, Z. He, R. Shahbazian-Yassar, W. Huang and T. Yu, High-rate, *Energy Storage Mater.*, 2018, **14**, 169–178.
4 R. Schmuch, R. Wagner, G. Hörpel, T. Placke and M. Winter, *Nat. Energy*, 2018, **3**, 267–278.
5 X. Chi, M. Li, J. Di, P. Bai, L. Song, X. Wang, F. Li, S. Liang, J. Xu and J. Yu, *Nature*, 2021, **592**, 551–557.
6 Y. Zhang, Y. Wu, H. Li, J. Chen, D. Lei and C. Wang, *Nat. Commun.*, 2022, **13**, 1297.
7 S. Li, F. Wu, T. Chen, K. Kang, R. Guo, C. Liu, Y. Niu, A. Gao, R. Zhao, X. Wang, Y. Bai and C. Wu, *Energy Mater. Adv.*, 2025, **6**, 168.
8 M. F. Roslan, P. R. Satpathy, T. Prasankumar, V. K. Ramachandaramurthy, M. Mansor and S. L. Walker, *J. Energy Storage*, 2025, **123**, 116808.
9 B. Zhang, J. Ma, Y. Zhao, T. Li, J. Yang, Z. Zhang, S. Wei and G. Zhou, *Rare Met.*, 2024, **43**, 942–970.
10 K. Yoon, S. Lee, K. Oh and K. Kang, *Adv. Mater.*, 2022, **34**, e2104666.
11 L. Li, W. Liu, H. Dong, Q. Gui, Z. Hu, Y. Li and J. Liu, *Adv. Mater.*, 2021, **33**, e2004959.
12 S. Huo, L. Wang, B. Su, W. Xue, Y. Wang, H. Zhang, M. Li, J. Qiu, H. Xu and X. He, *Adv. Mater.*, 2024, **36**, 2411757.
13 M. Liu, A. Song, X. Zhang, J. Wang, Y. Fan, G. Wang, H. Tian, Z. Ma and G. Shao, *Nano Energy*, 2025, **136**, 110749.
14 A. Fu, C. Wang, J. Peng, M. Su, F. Pei, J. Cui, X. Fang, J. F. Li and N. Zheng, *Adv. Funct. Mater.*, 2021, **31**, 2009805.
15 A. Pei, G. Zheng, F. Shi, Y. Li and Y. Cui, *Nano Lett.*, 2017, **17**, 1132–1139.
16 Z. Guo, J. Wang, X. Li, Z. Wang, H. Guo, W. Peng, G. Yan, G. Li, X. Zhang, N. Wang, J. Yang and X. Huang, *Electrochem. Energy Rev.*, 2025, **8**, 8.
17 X. Pu, S. Zhang, D. Zhao, Z. Xu, Z. Chen and Y. Cao, *Electrochem. Energy Rev.*, 2024, **7**, 21.
18 X. Liang, Q. Pang, I. R. Kochetkov, M. S. Sempere, H. Huang, X. Sun and L. F. Nazar, *Nat. Energy*, 2017, **2**, 17119.

Open Access Article. Published on 23 December 2025. Downloaded on 1/13/2026 8:44:30 PM.
This article is licensed under a Creative Commons Attribution-NonCommercial 3.0 Unported Licence.

19 Y. Liu, D. Gao, H. Xiang, X. Feng and Y. Yu, *Energy Fuels*, 2021, **35**, 12921–12937.
20 Z. L. Brown, S. Jurng and B. L. Lucht, *J. Electrochem. Soc.*, 2017, **164**, A2186–A2189.
21 J. Liu, Z. Bao, Y. Cui, E. J. Dufek, J. B. Goodenough, P. Khalifah, Q. Li, B. Y. Liaw, P. Liu, A. Manthiram, Y. S. Meng, V. R. Subramanian, M. F. Toney, V. V. Viswanathan, M. S. Whittingham, J. Xiao, W. Xu, J. Yang, X. Yang and J. Zhang, *Nat. Energy*, 2019, **4**, 180–186.
22 J. Lin, C. Ma, C. Li, X. Zou, W. Chen, J. Zhou and P. Lian, *ACS Appl. Mater. Interfaces*, 2025, **17**, 33191–33198.
23 W. Bao, R. Wang, B. Li, C. Qian, Z. Zhang, J. Li and F. Liu, *J. Mater. Chem. A*, 2021, **9**, 2957–2984.
24 V. Pande and V. Viswanathan, *ACS Energy Lett.*, 2019, **4**, 2952–2959.
25 X. Zhang, L. J. Huang, G. B. Yang, J. P. Song, G. H. Cong, S. S. Liu, Y. T. Huang, Z. Y. Liu and L. Geng, *Electrochim. Acta*, 2024, **498**, 144633.
26 Y. Xu, B. Yu, Y. Wang, F. Tan, G. Cheng, W. Yang, H. Gao and Z. Zhang, *Electrochim. Acta*, 2022, **435**, 141337.
27 X. Shen, R. Zhang, P. Shi, X. Chen and Q. Zhang, *Adv. Energy Mater.*, 2021, **11**, 2003416.
28 A. A. Assegie, C. Chung, M. Tsai, W. Su, C. Chen and B. Hwang, *Nanoscale*, 2019, **11**, 2710–2720.
29 A. B. Gunnarsdóttir, C. V. Amanchukwu, S. Menkin and C. P. Grey, *J. Am. Chem. Soc.*, 2020, **142**, 20814–20827.
30 D. Lin, Y. Liu, Y. Li, Y. Li, A. Pei, J. Xie, W. Huang and Y. Cui, *Nat. Chem.*, 2019, **11**, 382–389.
31 P. Zhu, D. Gastol, J. Marshall, R. Sommerville, V. Goodship and E. Kendrick, *J. Power Sources*, 2021, **485**, 229321.
32 M. J. Lain, J. Brandon and E. Kendrick, *Batteries*, 2019, **5**, 64.
33 B. A. Johnson and R. E. White, *J. Power Sources*, 1998, **70**, 48–54.
34 I. T. Røe and S. K. Schnell, *J. Mater. Chem. A*, 2021, **9**, 1142–1148.
35 J. Lee, J. Kim, D. G. Lee, D. Son, J. Lee, S. Kim, S. Han, N. Choi, T. K. Lee and J. Lee, *Chem. Eng. J.*, 2024, **499**, 156296.
36 C. Park, J. Kim, W. Lim and J. Lee, *Exploration*, 2024, **4**, 20210255.
37 T. Fuchs, C. G. Haslam, A. C. Moy, C. Lerch, T. Krauskopf, J. Sakamoto, F. H. Richter and J. Janek, *Adv. Energy Mater.*, 2022, **12**, 2201125.
38 L. Liu and J. Wang, *Nano Lett.*, 2023, **23**, 10251–10258.
39 Y. Li, Y. Li, A. Pei, K. Yan, Y. Sun, C. Wu, L. Joubert, R. Chin, A. L. Koh, Y. Yu, J. Perrino, B. Butz, S. Chu and Y. Cui, *Science*, 2017, **358**, 506–510.
40 Y. Gu, H. Xu, X. Zhang, W. Wang, J. He, S. Tang, J. Yan, D. Wu, M. Zheng, Q. Dong and B. Mao, *Angew. Chem., Int. Ed.*, 2019, **58**, 3092–3096.
41 X. Cheng, R. Zhang, C. Zhao and Q. Zhang, *Chem. Rev.*, 2017, **117**, 10403–10473.
42 K. Ishikawa, S. Harada, M. Tagawa and T. Ujihara, *ACS Appl. Mater. Interfaces*, 2020, **12**, 9341–9346.
43 Q. Zhao, Y. Deng, N. W. Utomo, J. Zheng, P. Biswal, J. Yin and L. A. Archer, *Nat. Commun.*, 2021, **12**, 6034.
44 G. Li, D. Shi, Z. Hao, Y. Lu, Q. Zhao, Z. Yan, W. Xie, X. Meng and J. Chen, *J. Phys. Chem. C*, 2023, **127**, 16297–16303.
45 Y. Kim, S. H. Kwon, H. Noh, S. Yuk, H. Lee, H. S. Jin, J. Lee, J. Zhang, S. G. Lee, H. Guim and H. Kim, *Energy Storage Mater.*, 2019, **19**, 154–162.
46 J. Y. Kim, O. B. Chae, M. Wu, E. Lim, G. Kim, Y. J. Hong, W. Jung, S. Choi, D. Y. Kim, I. Gereige, J. Suk, Y. Kang and H. Jung, *Nano Energy*, 2021, **82**, 105736.
47 J. Zhan, L. Deng, Y. Liu, M. Hao, Z. Wang, L. T. Dong, Y. Yang, K. Song, D. Qi, J. Wang, S. Wang, H. Liu, W. Zhou and H. Chen, *Adv. Mater.*, 2025, **37**, 2413420.
48 Z. Hao, G. Li, C. Zheng, X. Liu, S. Wu, H. Li, K. Zhang, Z. Yan and J. Chen, *Angew. Chem., Int. Ed.*, 2024, **63**, e202407064.
49 Y. Liu, C. Sun, Y. Lu, X. Lin, M. Chen, Y. Xie, C. Lai and W. Yan, *Chem. Eng. J.*, 2023, **451**, 138570.
50 D. Li, Y. Gao, C. Xie and Z. Zheng, *Appl. Phys. Rev.*, 2022, **9**, 011424.
51 C. Shan, Z. Qin, Y. Xie, X. Meng, J. Chen, Y. Chang, R. Zang, L. Wan and Y. Huang, *Carbon*, 2023, **204**, 367–376.
52 J. Lu, Z. Ma, Y. Wang, W. Dai, X. Cheng, J. Zuo, H. Lei and Z. Fu, *Small*, 2024, **20**, e2406359.
53 K. Yan, Z. Lu, H. Lee, F. Xiong, P. Hsu, Y. Li, J. Zhao, S. Chu and Y. Cui, *Nat. Energy*, 2016, **1**, 16010.
54 J. Du, W. Wang, M. Wan, X. Wang, G. Li, Y. Tan, C. Li, S. Tu and Y. Sun, *Adv. Energy Mater.*, 2021, **11**, 2102259.
55 J. Cao, Y. Shi, A. Gao, G. Du, M. Dilxat, Y. Zhang, M. Cai, G. Qian, X. Lu, F. Xie, Y. Sun and X. Lu, *Nat. Commun.*, 2024, **15**, 1354.
56 H. Jo, J. Lee, E. Kwon, S. Yu, B. G. Kim, S. Park, J. Moon, M. J. Ko and H. Lim, *ACS Nano*, 2024, **18**, 35718–35728.
57 X. Duan, J. Sun, L. Shi, S. Dong and G. Cui, *Interdiscip. Mater.*, 2025, **4**, 217–234.
58 R. Guan, S. Liu, C. Wang, Y. Yang, D. Lu and X. Bian, *Chem. Eng. J.*, 2021, **425**, 130177.
59 H. Wang, Y. Mao, P. Xu, Y. Ding, H. Yang, J. Li, Y. Gu, J. Han, L. Zhang and B. Mao, *Energy Environ. Sci.*, 2025, **18**, 2622–2633.
60 K. Wang, J. Hu, T. Chen, W. Zhang, Z. Deng, Q. Chen, K. Wang and J. Wu, *J. Energy Storage*, 2024, **89**, 111879.
61 B. Hubert, Y. Nikodimos, B. J. Hwang and J. P. Chu, *J. Power Sources*, 2024, **589**, 233660.
62 J. Seo, J. Lim, H. Chang, J. Lee, J. Woo, I. Jung, Y. Kim, B. Kim, J. Moon and H. Lee, *Small*, 2024, **20**, e2402988.
63 Z. T. Wondimkun, W. A. Tegegne, J. Shi-Kai, C. Huang, N. A. Sahalie, M. A. Weret, J. Hsu, P. Hsieh, Y. Huang, S. Wu, W. Su and B. J. Hwang, *Energy Storage Mater.*, 2021, **35**, 334–344.
64 J. Zhu, Y. Wu, X. Huang, L. Huang, M. Cao, G. Song, X. Guo, X. Sui, R. Ren and J. Chen, *Nano Energy*, 2019, **62**, 883–889.

 © 2026 The Author(s). Published by the Royal Society of Chemistry

Open Access Article. Published on 23 December 2025. Downloaded on 1/13/2026 8:44:30 PM.
This article is licensed under a Creative Commons Attribution-NonCommercial 3.0 Unported Licence.

65 Y. Zhou, P. Wang, K. Wang, X. Fang, W. Li, J. Nai, Y. Liu, Y. Wang, S. Zou, H. Yuan, X. Tao and J. Luo, *Adv. Funct. Mater.*, 2025, **35**, 2424022.
66 B. Zhou, A. Bonakdarpour, I. Stoševski, B. Fang and D. P. Wilkinson, *Prog. Mater. Sci.*, 2022, **130**, 100996.
67 Y. Liu, Y. Li, J. Sun, Z. Du, X. Hu, J. Bi, C. Liu, W. Ai and Q. Yan, *Nano Res. Energy*, 2023, **2**, e9120048.
68 P. Du, C. Yuan, X. Cui, K. Zhang, Y. Yu, X. Ren, X. Zhan and S. Gao, *J. Mater. Chem. A*, 2022, **10**, 8424–8431.
69 J. Teng, X. Tang, H. Li, Q. Wu, D. Zhao and J. Li, *J. Power Sources*, 2022, **540**, 231642.
70 X. F. Tan, Q. Gu, D. Qu, A. X. B. Yong, W. Yang, S. D. McDonald, S. Matsumura and K. Nogita, *Acta Mater.*, 2020, **201**, 341–349.
71 S. J. Liu, K. J. Jiao and J. H. Yan, *Energy Storage Mater.*, 2023, **54**, 689–712.
72 X. Zhang, S. Huang, M. Xiao, S. J. Wang, Y. Z. Meng and D. M. Han, *J. Power Sources*, 2025, **631**, 236200.
73 S. T. Wang, Y. Liu, J. R. Huang, S. Z. Liu, S. L. Li, M. R. Liu, Z. C. Ma, T. F. Yang, Y. J. Yang and S. Y. Gao, *Nano Energy*, 2025, **138**, 110843.
74 J. Q. Cao, W. X. Chen, A. S. Gao, D. Muhtar, G. Y. Du, G. Y. Qian, X. Y. Lu, F. Y. Xie, Y. Sun and X. Lu, *Angew. Chem., Int. Ed.*, 2025, **64**, e202413065.
75 V. P. Nguyen, H. C. Shim, Y. Byeon, J. Kim and S. Lee, *Adv. Sci.*, 2025, **12**, e2416426.
76 S. Qian, C. Xing, M. Zheng, Z. Su, H. Chen, Z. Wu, C. Lai and S. Zhang, *Adv. Energy Mater.*, 2022, **12**, 2103480.
77 M. Gao, Q. Dong, M. Yao, X. Wang, J. Li, W. Zhang, H. Huang, H. Guo, Z. Sun, Q. Chen, X. Han and W. Hu, *Adv. Funct. Mater.*, 2024, **34**, 2401442.
78 Z. Liu, L. Sun, X. Liu and Q. Lu, *Chem. – Eur. J.*, 2024, **30**, e202402032.
79 B. Li, Y. Chao, M. Li, Y. Xiao, R. Li, K. Yang, X. Cui, G. Xu, L. Li, C. Yang, Y. Yu, D. P. Wilkinson and J. Zhang, *Electrochem. Energy Rev.*, 2023, **6**, 7.
80 L. Song, D. Ning, Y. Chai, M. Ma, G. Zhang, A. Wang, H. Su, D. Hao, M. Zhu, J. Zhang, D. Zhou, J. Wang and Y. Li, *Small Methods*, 2023, **7**, 2300168.
81 B. Han, Y. Zou, G. Xu, S. Hu, Y. Kang, Y. Qian, J. Wu, X. Ma, J. Yao, T. Li, Z. Zhang, H. Meng, H. Wang, Y. Deng, J. Li and M. Gu, *Energy Environ. Sci.*, 2021, **14**, 4882–4889.
82 B. Wu, C. Chen, L. H. J. Raijmakers, J. Liu, D. L. Danilov, R. Eichel and P. H. L. Notten, *Energy Storage Mater.*, 2023, **57**, 508–539.
83 C. Wang, R. Odstrcil, J. Liu and W. Zhong, *J. Energy Chem.*, 2022, **73**, 248–258.
84 Y. Wu, C. Wang, C. Wang, Y. Zhang, J. Liu, Y. Jin, H. Wang and Q. Zhang, *Mater. Horiz.*, 2024, **11**, 388–407.
85 N. Li, G. Kang, S. Huang, J. Biao, Y. Liu, F. Kang and Y. Cao, *ACS Appl. Mater. Interfaces*, 2025, **17**, 36627–36638.
86 S. Miao, Y. Jia, Z. Deng, Y. Deng, R. Chen, X. Zhang, C. Xu, M. Yao and W. Cai, *Tungsten*, 2024, **6**, 212–229.
87 Q. Zhang, J. Luan, Y. Tang, X. Ji, S. Wang and H. Wang, *J. Mater. Chem. A*, 2018, **6**, 18444–18448.
88 R. U. R. Sagar, M. W. Fazal, A. Durajski, M. W. Khan, N. Mahmood and Y. Chen, *Nano Lett.*, 2025, **25**, 10970–10976.
89 S. T. Oyakhire, W. Zhang, A. Shin, R. Xu, D. T. Boyle, Z. Yu, Y. Ye, Y. Yang, J. A. Raiford, W. Huang, J. R. Schneider, Y. Cui and S. F. Bent, *Nat. Commun.*, 2022, **13**, 3986.
90 V. P. Nguyen, H. C. Shim, Y. W. Byeon, J. H. Kim and S. M. Lee, *Adv. Sci.*, 2025, **12**, 2416426.
91 Y. Liu, X. Meng, Y. Shi, J. Qiu and Z. Wang, *Adv. Mater.*, 2023, **35**, 2305386.
92 K. Vishweswariah, N. G. Ningappa, M. D. Bouguern, A. Kumar M R, M. B. Armand and K. Zaghib, *Adv. Energy Mater.*, 2025, 2501883.
93 H. Song, J. Lee, M. Sagong, J. Jeon, Y. Han, J. Kim, H. G. Jung, J. S. Yu, J. Lee and I. D. Kim, *Adv. Mater.*, 2024, **36**, 2407381.
94 Y. Liu, Y. Zhen, T. Li, F. Bettels, T. He, M. Peng, Y. Liang, F. Ding and L. Zhang, *Small*, 2020, **16**, 2004770.
95 C. Chen, Q. Liang, G. Wang, D. Liu and X. Xiong, *Adv. Funct. Mater.*, 2022, **32**, 2107249.
96 A. Hu, W. Chen, X. Du, Y. Hu, T. Lei, H. Wang, L. Xue, Y. Li, H. Sun, Y. Yan, J. Long, C. Shu, J. Zhu, B. Li, X. Wang and J. Xiong, *Energy Environ. Sci.*, 2021, **14**, 4115–4124.
97 Q. Ran, H. Zhao, J. Liu, L. Li, Q. Hu, J. Song, X. Liu and S. Kormarneni, *J. Energy Chem.*, 2023, **83**, 612–621.
98 S. Chen, C. Pan, Q. Wang, J. L. Luo and X. Z. Fu, *Adv. Funct. Mater.*, 2024, **34**, 2409812.
99 Z. Cao, H. Chen, Z. Du, J. Gu, Q. Zhu, B. Li and S. Yang, *Adv. Energy Mater.*, 2022, **12**, 2201189.
100 C. Chang, Y. Yao, R. Li, Z. H. Guo, L. Li, C. Pan, W. Hu and X. Pu, *Nano Energy*, 2022, **93**, 106871.
101 S. Gao, F. Sun, N. Liu, H. Yang and P. Cao, *Mater. Today*, 2020, **40**, 140–159.
102 Y. Nikodimos, W. Su, K. N. Shitaw, S. Jiang, L. H. Abrha, M. A. Weret, S. K. Merso, T. M. Hagos, C. Huang, K. Lakshmanan, W. Huang, C. Chang, J. Lin, S. Wu, C. Yang and B. J. Hwang, *Energy Storage Mater.*, 2023, **61**, 102861.
103 S. Li, J. Huang, Y. Cui, S. Liu, Z. Chen, W. Huang, C. Li, R. Liu, R. Fu and D. Wu, *Nat. Nanotechnol.*, 2022, **17**, 613–621.
104 C. Chen, J. Zhang, B. Hu, Q. Liang and X. Xiong, *Nat. Commun.*, 2023, **14**, 4018.
105 H. Wang, Y. Peng, R. Tamate, K. Nishikawa and S. Nakanishi, *J. Power Sources*, 2025, **641**, 236801.
106 W. Lu, L. Sun, Y. Zhao, T. Wu, L. Cong, J. Liu, Y. Liu and H. Xie, *Energy Storage Mater.*, 2021, **34**, 241–249.
107 M. Pang, Z. Jiang, C. Luo, Z. Yao, T. Fu, T. Pan, Q. Guo, Y. Li, S. Xiong, C. Zheng, W. Sun, G. Zhou and S. Liu, *Energy Environ. Sci.*, 2024, **17**, 7699–7711.
108 D. Han, Z. Wang, S. Chen, J. Zhou, S. Chen, M. Wang, D. Wu, X. Meng, C. W. Bielawski and J. Geng, *Small*, 2024, **20**, 2405453.

Open Access Article. Published on 23 December 2025. Downloaded on 1/13/2026 8:44:30 PM.
This article is licensed under a Creative Commons Attribution-NonCommercial 3.0 Unported Licence.

109 S. Zhou, Y. Zhang, S. Chai, I. Usman, Y. Qiao, S. Luo, X. Xie, J. Chen, S. Liang, A. Pan and H. Zhou, *Chem. Eng. J.*, 2021, **404**, 126508.
110 Y. Cheng, J. Chen, Y. Chen, X. Ke, J. Li, Y. Yang and Z. Shi, *Energy Storage Mater.*, 2021, **38**, 276–298.
111 Y. Wang, J. Tan, Z. Li, L. Ma, Z. Liu, M. Ye and J. Shen, *Energy Storage Mater.*, 2022, **53**, 156–182.
112 S. Park, H. J. Jin and Y. S. Yun, *Adv. Mater.*, 2020, **32**, 2002193.
113 C. Zhang, R. Lyu, W. Lv, H. Li, W. Jiang, J. Li, S. Gu, G. Zhou, Z. Huang, Y. Zhang, J. Wu, Q. H. Yang and F. Kang, *Adv. Mater.*, 2019, **31**, 1904991.
114 C. Yang, Y. Yin, S. Zhang, N. Li and Y. Guo, *Nat. Commun.*, 2015, **6**, 8058.
115 S. K. Park, D. Copic, T. Z. Zhao, A. Rutkowska, B. Wen, K. Sanders, R. He, H. Kim and M. De Volder, *ACS Nano*, 2023, **17**, 14658–14666.
116 W. Shin and A. Manthiram, *ACS Appl. Mater. Interfaces*, 2022, **14**, 17454–17460.
117 Q. Chen, Y. Yang, H. Zheng, Q. Xie, X. Yan, Y. Ma, L. Wang and D. Peng, *J. Mater. Chem. A*, 2019, **7**, 11683–11689.
118 W. Chen, S. Li, C. Wang, H. Dou and X. Zhang, *Energy Environ. Mater.*, 2023, **6**, e12412.
119 J. Kim, S. Lee, J. Kim, J. Park, H. Lee, J. Kwon, S. Sun, J. Choi, U. Paik and T. Song, *Carbon Energy*, 2024, **6**, e610.
120 S. K. Park, S. Kim, R. He, K. Sanders, U. Hwang, Z. An, M. Hamidinejad, J. W. Kim and M. De Volder, *Small*, 2025, **21**, 2501292.
121 T. Zhao, S. Li, F. Liu, Z. Wang, H. Wang, Y. Liu, X. Tang, M. Bai, M. Zhang and Y. Ma, *Energy Storage Mater.*, 2022, **45**, 796–804.
122 H. Liu, E. Wang, Q. Zhang, Y. Ren, X. Guo, L. Wang, G. Li and H. Yu, *Energy Storage Mater.*, 2019, **17**, 253–259.
123 F. Shen, F. Zhang, Y. Zheng, Z. Fan, Z. Li, Z. Sun, Y. Xuan, B. Zhao, Z. Lin, X. Gui, X. Han, Y. Cheng and C. Niu, *Energy Storage Mater.*, 2018, **13**, 323–328.
124 N. Li, T. Jia, Y. Liu, Y. Ouyang, Y. Lv, G. Zhong, Y. Wang, B. Sun, S. Lu, S. Huang, F. Kang and Y. Cao, *Mater. Today Energy*, 2023, **36**, 101341.
125 Y. Ma, X. Ma, J. Bai, W. Xu, H. Zhong, Z. Liu, S. Xiong, L. Yang and H. Chen, *Small*, 2023, **19**, 2301731.
126 S. Kim, M. Lee, S. Oh and W. Ryu, *Chem. Eng. J.*, 2023, **474**, 145447.
127 G. Guo, K. Zhang, K. Zhu, P. Yang, Z. Shao, S. Liu, L. Lin, W. Zhuang, P. Xue, Q. Zhang and Y. Yao, *Adv. Funct. Mater.*, 2024, **34**, 2402490.
128 Q. Yun, Y. B. He, W. Lv, Y. Zhao, B. Li, F. Kang and Q. H. Yang, *Adv. Mater.*, 2016, **28**, 6932–6939.
129 W. Liu, D. Lin, A. Pei and Y. Cui, *J. Am. Chem. Soc.*, 2016, **138**, 15443–15450.
130 L. Qin, Y. Wu, M. Shen, B. Song, Y. Li, S. Sun, H. Zhang, C. Liu and J. Chen, *Energy Storage Mater.*, 2022, **44**, 278–284.
131 S. H. Wang, Y. X. Yin, T. T. Zuo, W. Dong, J. Y. Li, J. L. Shi, C. H. Zhang, N. W. Li, C. J. Li and Y. G. Guo, *Adv. Mater.*, 2017, **29**, 1703721–1703729.
132 H. Shen, P. Tang, Q. Wei, Y. Zhang, T. Yu, H. Yang, R. Zhang, K. Tai, J. Tan, S. Bai and F. Li, *Small*, 2023, **19**, 2206000.
133 Z. Li, X. Huang, L. Kong, N. Qin, Z. Wang, L. Yin, Y. Li, Q. Gan, K. Liao, S. Gu, T. Zhang, H. Huang, L. Wang, G. Luo, X. Cheng and Z. Lu, *Energy Storage Mater.*, 2022, **45**, 40–47.
134 H. Li, G. Wang, J. Hu, J. Li, J. Huang and S. Xu, *Energy Environ. Mater.*, 2024, **7**, e12768.
135 J. Qi, Y. Feng, J. Yu, H. Wang, Z. Wu, J. Zhao, Y. Jiang, J. Liu, Y. Li, L. Zhou, K. Zhang and J. Chen, *Energy Storage Mater.*, 2025, **77**, 104176.
136 W. Guan, Y. Lv, C. Ma, Q. Zhang, A. Wei and X. Liu, *Mater. Chem. Front.*, 2023, **7**, 315–324.
137 X. He, D. Bresser, S. Passerini, F. Baakes, U. Krewer, J. Lopez, C. T. Mallia, Y. Shao-Horn, I. Cekic-Laskovic, S. Wiemers-Meyer, F. A. Soto, V. Ponce, J. M. Seminario, P. B. Balbuena, H. Jia, W. Xu, Y. Xu, C. Wang, B. Horstmann, R. Amine, C. Su, J. Shi, K. Amine, M. Winter, A. Latz and R. Kostecki, *Nat. Rev. Mater.*, 2021, **6**, 1036–1052.
138 Z. Yubo, C. Jianzhong, Z. Zhihao, Z. Haitao and Q. Ke, *Mater. Sci. Eng., A*, 2005, **406**, 286–292.
139 Y. Luo, Z. Zhang, B. Li, M. Gao, Y. Qiu and M. He, *JOM*, 2017, **69**, 2640–2643.
140 J. Q. Wang and G. Xiao, *J. Appl. Phys.*, 1996, **79**, 5587–5589.
141 M. Miura, Y. Oshikiri, A. Sugiyama, R. Morimoto, I. Mogi, M. Miura, S. Takagi, Y. Yamauchi and R. Aogaki, *Sci. Rep.*, 2017, **7**, 45511.
142 Y. D. Yu, Z. L. Song, H. L. Ge and G. Y. Wei, *Surf. Eng.*, 2014, **30**, 83–86.
143 O. Aaboubi, A. Y. A. Omar, A. Franczak and K. Msellak, *J. Electroanal. Chem.*, 2015, **737**, 226–234.
144 L. M. A. Monzon and J. M. D. Coey, *Electrochem. Commun.*, 2014, **42**, 38–41.
145 D. Lin, Y. Liu and Y. Cui, *Nat. Nanotechnol.*, 2017, **12**, 194–206.
146 Q. Cheng, L. Wei, Z. Liu, N. Ni, Z. Sang, B. Zhu, W. Xu, M. Chen, Y. Miao, L. Chen, W. Min and Y. Yang, *Nat. Commun.*, 2018, **9**, 2942.
147 L. Yu, J. Wang and Z. J. Xu, *Small Struct.*, 2021, **2**, 2000043.
148 K. Shen, Z. Wang, X. Bi, Y. Ying, D. Zhang, C. Jin, G. Hou, H. Cao, L. Wu, G. Zheng, Y. Tang, X. Tao and J. Lu, *Adv. Energy Mater.*, 2019, **9**, 1900260.
149 M. Bae, M. Kang and Y. Piao, *Adv. Funct. Mater.*, 2025, **35**, 2421952.
150 Z. Gao, Y. Schwab, Y. Zhang, N. Song and X. Li, *Adv. Funct. Mater.*, 2018, **28**, 1800563.
151 S. Zhou, X. Meng, C. Fu, J. Chen, Y. Chen, D. Xu, S. Lin, C. Han, Z. Chang and A. Pan, *Small*, 2023, **19**, 2207764.
152 M. Liu, J. Ma, X. Zhang, J. Wang, Y. Fan, A. Song, G. Shao and Z. Ma, *Adv. Funct. Mater.*, 2025, **35**, 2416527.

 © 2026 The Author(s). Published by the Royal Society of Chemistry

Open Access Article. Published on 23 December 2025. Downloaded on 1/13/2026 8:44:30 PM.
This article is licensed under a Creative Commons Attribution-NonCommercial 3.0 Unported Licence.

153 H. Chen, J. Hu, H. Li, J. Zhang, Q. Chen, G. Hou and Y. Tang, *Small*, 2024, **20**, 2307598.
154 M. Sheikholeslami and M. Gorji-Bandpy, *Powder Technol.*, 2014, **256**, 490–498.
155 J. Zhang, H. Chen, M. Wen, K. Shen, Q. Chen, G. Hou and Y. Tang, *Adv. Funct. Mater.*, 2022, **32**, 2110110.
156 F. A. Garcés-Pineda, M. Blasco-Ahicart, D. Nieto-Castro, N. López and J. R. Galán-Mascarós, *Nat. Energy*, 2019, **4**, 519–525.
157 J. Feng, C. Shi, X. Zhao, Y. Zhang, S. Chen, X. Cheng and J. Song, *Adv. Mater.*, 2024, **36**, 2414047.
158 C. Y. Zhang, C. Zhang, G. W. Sun, J. L. Pan, L. Gong, G. Z. Sun, J. J. Biendicho, L. Balcells, X. L. Fan, J. R. Morante, J. Y. Zhou and A. Cabot, *Angew. Chem., Int. Ed.*, 2022, **61**, e202211570.
159 G. Sun, C. Y. Zhang, M. Jin, J. Li, X. Pan, A. Cabot, G. Sun and J. Y. Zhou, *J. Am. Chem. Soc.*, 2025, **147**, 27251–27264.